1961

Experimental Determination of the Thermal Conductivity and Peltier Tensors in a Single Crystal of Zinc at Liquid Helium Temperature.

Nadim Hanna Zebouni
Louisiana State University and Agricultural & Mechanical College

EXPERIMENTAL DETERMINATION OF THE THERMAL CONDUCTIVITY AND PELTIER TENSORS IN A SINGLE CRYSTAL OF ZINC AT LIQUID HELIUM TEMPERATURE

A Dissertation

Submitted to the Graduate Faculty of the
Louisiana State University and
Agricultural and Mechanical College
in partial fulfillment of the
requirements for the degree of
Doctor of Philosophy

in

The Department of Physics and Astronomy

by
Nadim H. Zebouni
M.Sc. University of Paris, France, 1955
January, 1961

ACKNOWLEDGMENT

The author wishes to express his appreciation and gratitude to Dr. J. M. Reynolds for his guidance and direction of this work. He would also like to express his deep gratitude to Dr. Claude G. Grenier without whose help this work would not have been possible. To Dr. C. J. Bergeron the author gives sincere thanks for his help and direction of the early part of this work. To Dr. L. Morris and Mr. L. Edelen he expresses his appreciation for their many and valuable advices.

TABLE OF CONTENTS

LIST OF FIGURES

ABSTRACT

The variation of the thermal resistance, Righi-Leduc, Peltier and Ettingshausen effects, at liquid helium temperatures, in magnetic fields up to 10 Kilogauss has been investigated. The measurements were taken with either a constant heat current or a constant electric current flowing perpendicular to the hexagonal axis. The magnetic field was parallel to the hexagonal axis.

The magnetoresistance, Hall effect, thermoelectric power and Ettingshausen-Nernst effect were measured in the same crystal, in the same conditions.

The Righi-Leduc effect is found to change sign at 5400 gauss. Oscillations of de Haas-van Alphen type were found, with a period $P = 6.14 \times 10^{-5}$ gauss^{-1}. The Ettingshausen effect is found to be purely oscillatory with $P = 6.45 \times 10^{-5}$ gauss^{-1}. The amplitude of the oscillations seem to increase linearly with the magnetic field strength. The Peltier effect shows oscillations with $P = 6.28 \times 10^{-5}$ gauss^{-1}, superimposed on a strong linear monotonic increase whose slope is -.24 deg-cm/amp/Kgauss. A phase inversion of the oscillations is observed for $H < 5$ Kgauss, similar to what has been already observed in the thermoelectric power oscillations.

From the comparison or the Hall and Righi-Leduc effects, an apparent transverse Lorenz ratio is computed. Similarly, from comparison of the

thermal and electrical magnetoresistance effects an apparent longitudinal Lorenz ratio is computed. Their behavior is compared with theory and with previous results found in the literature.

An extrapolation gives an estimate of the lattice conductivity of zinc at $2^{o}K$, equal to .02 watt/deg-cm.

The thermoelectric power and Ettingshausen-Nernst results are compared respectively with the Peltier and Ettingshausen results in the light of the Onsager Theorem. An excellent agreement with the theory is found.

The two thermoelectric coefficients ϵ''_{11} and ϵ''_{21}, defined by the equation,

$$J_i = \sigma_{ik}E_k^* - \epsilon''_{ik}G_k \qquad i,k = 1,2,$$

are computed and their behavior analyzed in the light of recent theories.

CHAPTER I

INTRODUCTION

1. Irreversible Thermodynamics and the Onsager Theorem.*

The thermomagnetic and galvanomagnetic effects whose measurements are the subject of this work cannot be expressed in terms of equilibrium states. They are processes and the problem one is confronted with is that of the rates of these physical processes. Consequently the thermostatic theory and the equilibrium statistical mechanics are not applicable here. For these irreversible processes, one must turn to the theory of "Irreversible Thermodynamics" and to the nonequilibrium statistical mechanics. Consequently, we shall give here a brief account of the fundamental postulate of this theory, define the appropriate quantities that describe irreversible processes and in term of these, state the Onsager Theorem.

The theory of nonequilibrium statistical mechanics is based on the two postulates of the equilibrium theory, plus the additional postulate of time symmetry of physical laws. This additional postulate states that: All the laws of physics remain unchanged if the time t is everywhere replaced by its negative -t and if simultaneously the

---

*This follows closely the treatment by H. B. Callen, "Thermodynamics," Chap. 16, John Wiley and Sons, Inc., New York, 1960.

external magnetic field H_e is replaced by its negative $-H_e$. The most practically significant result of nonequilibrium thermodynamics is the Onsager reciprocity theorem, which expresses a certain symmetry in the response of two simultaneously occurring processes.

Preparatory to our statement of the Onsager theorem, we define certain quantities that appropriately describe irreversible processes. Basically we require two types of parameters: one to describe the "force" that drives a process and one to describe the response to this force.

The processes of most general interest occur in continuous systems, such as the flow of energy in a bar with a continuous temperature gradient. However, to suggest the proper way to choose parameters in such continuous systems, we first consider the relatively simple case of a discrete system. A typical process in a discrete system would be the flow of energy from one homogeneous subsystem to another through an infinitely thin diathermal partition.

Consider a composite system composed of two subsystems. An extensive parameter has values X_k and X_k' in the two subsystems, and the closure condition requires that

$$X_k + X_k' = X_k^o, \text{ a constant}$$

if X_k and X_k' are unconstrained, their equilibrium values are determined by the vanishing of the quantity,

$$F_k = \left(\frac{\partial S^o}{\partial X_k}\right)_{X_k^o} = \left(\frac{\partial (S+S')}{\partial X_k}\right)_{X_k^o} = \frac{\partial S}{\partial X_k} - \frac{\partial S}{\partial X_k'} = f_k - f_k' \qquad (1)$$

where S is the entropy. Thus, if F_k is zero, the system is in equilibrium, but if F_k is nonzero an irreversible process occurs, taking the system

toward the equilibrium state. The quantity F_k, which is the difference in the entropy-representation intensive parameters, $f_k - f_k'$, acts as a "generalized force" which "drives" the process. Such generalized forces are called <u>affinities</u>.

For definiteness, consider two systems separated by a diathermal wall, and let X_k be the energy U. Then the affinity is,

$$F_k = \left(\frac{\partial S^\circ}{\partial U}\right)_{U^\circ} = \frac{1}{T} - \frac{1}{T'} \ . \tag{2}$$

No heat flows across the diathermal wall if the difference in inverse temperatures vanishes. But a nonzero difference in inverse temperature, acting as a generalized force, drives a flow of heat between the subsystems. The extension of this example to a continuous system is seen by the method of local equilibrium, to yield for the affinity the gradient of $\frac{1}{T}$.

Similarly, if X_k is the volume, the affinity F_k is $\nabla\left(\frac{p}{T}\right)$ and if X_k is the number of electrons per unit volume the associated affinity is $\nabla\left(\frac{\mu}{T}\right)$ where μ is the electrochemical potential per particle. More generally, one has $F_k = \nabla f_k$.

We characterize the response to the applied force by the rate of change of the extensive parameter X_k. The flux J_k is then defined by

$$J_k = \frac{dX_k}{dt} \tag{3}$$

It is the relationship between fluxes and affinities that characterizes the rates of irreversible processes.

For certain systems, the fluxes at a given instant depend only on the values of the affinities at that instant. We call such systems Markoffian, and we restrict our attention to this type of system.

For a non-Markoffian system the fluxes may depend upon the values of the affinities at previous times as well as upon the values at the present time. In the electrical case, a pure resistor is a Markoffian system, whereas a circuit with capacitance or inductance is non-Markoffian. A non-Markoffian system has a "memory."

For a Markoffian system, by definition, each local flux depends only upon the instantaneous local affinities and upon the intensive local parameters. That is, in vector notation

$$J_k = J_k(F_o, \ldots F_j, \ldots, f_o, f_1, \ldots f_j \ldots) \tag{4}$$

It should be noted that we do not assume that each flux depends only on its own affinity but rather that each flux depends on <u>all</u> affinities.

Each flux J_k vanishes as the affinities vanish, so we can expand J_k in powers of the affinities with no constant term.

$$J_k = \sum_j L_{jk} F_j + \frac{1}{2!} \sum_i \sum_j L_{ijk} F_i F_j + \ldots \tag{5}$$

The functions L_{jk} are called kinetic coefficients. They are functions of the local intensive parameters.

For the purposes of the Onsager theorem, which we are about to enunciate, it is convenient to adopt a notation that exhibits the functional dependence of the kinetic coefficients on an externally applied magnetic field H_e, ignoring the dependence on the other intensive parameters.

$$L_{jk} = L_{jk}(H_e) \tag{6}$$

The Onsager theorem states that

$$L_{jk}(H_e) = L_{kj}(-H_e) \tag{7}$$

That is, the value of the kinetic coefficient L_{jk} measured in an

external magnetic field H_e is identical to the value of L_{kj} measured in the reversed magnetic field $-H_e$. The Onsager theorem states a symmetry between the linear effect of the j^{th} affinity on the k^{th} flux and the linear effect of the k^{th} affinity on the j^{th} flux, when these effects are measured in opposite magnetic fields.

A process that can be adequately described by the truncated approximate equations

$$J_k = \sum_j L_{jk} F_k \tag{8}$$

is called a linear Markoff process. The affinities that we commonly encounter in the laboratory are quite small in the sense of equation (5), so that all quadratic and higher-order terms in this equation can be neglected.

For the analysis of such processes the Onsager theorem is a particularly powerful tool, but is not restricted to this special class of systems.

2. The Dynamical Equations

Consider u, s, and J_n as the current densities of energy, entropy and number of electrons, respectively.

If the components of u and J_n are taken as fluxes, the associated affinities are the components of $\nabla(\frac{1}{T})$ and $-\nabla(\frac{\mu}{T})$, where T is the absolute temperature and μ the electrochemical potential per electron.

If instead we choose as fluxes the components of w^* and J_n, where

$$w^* = Ts = u - \mu J_n, \tag{9}$$

is the heat current, the associated affinities are the components of $\nabla(\frac{1}{T})$ and $-\frac{1}{T}\nabla(\mu)$.

In the case of the experiment the two independent quantities on which one had direct control were the electric current density

$$J = eJ_n \tag{10}$$

and the absolute heat current density w. The quantity e is a negative number.

We have here to comment briefly on the nature of the electrochemical potential of the electrons. We can consider μ as composed of two parts, a chemical portion μ_c and an electrical portion μ_e,

$$\mu = \mu_c + \mu_e. \tag{11}$$

If the charge on an electron is e (negative number), then μ_e is simply $e\phi$ where ϕ is the ordinary electrostatic potential. The chemical potential μ_c is a function of the temperature and of the electron concentration.

Restating these facts in terms of gradients, the electrochemical potential per unit charge is $-(\frac{1}{e})\mu$, its gradient $-(\frac{1}{e})\nabla\mu$ is the sum of the electric field $-(\frac{1}{e})\nabla\mu_e$ plus an effective driving force $-(\frac{1}{e})\nabla\mu_c$ arising from a concentration gradient. Thus,[1]

$$E^* = -\frac{1}{e}\nabla\mu = E - (\frac{1}{e})\nabla\mu_c \tag{12}$$

and it is important to note that the electrostatic potential E is the one that is directly measurable. We will return to this important distinction in Chapter III.

We can now write the dynamical equations for a 3-dimensional isotropic medium:

---

[1] H. B. Callen, Phys. Rev. 85, 16 (1952).

$$
\begin{aligned}
J_1 &= \sigma_{11}E_1^* + \sigma_{12}E_2^* + \sigma_{13}E_3^* - \epsilon''_{11}G_1 - \epsilon''_{12}G_2 - \epsilon''_{13}G_3 \\
J_2 &= \sigma_{21}E_1^* + \sigma_{22}E_2^* + \sigma_{23}E_3^* - \epsilon''_{21}G_1 - \epsilon''_{22}G_2 - \epsilon''_{23}G_3 \\
w_1^* &= -\pi''_{11}E_1^* - \pi''_{12}E_2^* - \pi''_{13}E_3^* + \lambda''_{11}G_1 + \lambda''_{12}G_2 + \lambda''_{13}G_3 \\
w_2^* &= -\pi''_{21}E_1^* - \pi''_{22}E_2^* - \pi''_{23}E_3^* + \lambda''_{21}G_1 + \lambda''_{22}G_2 + \lambda''_{23}G_3
\end{aligned}
\tag{13}
$$

where $G = \nabla T = T^2 \nabla (\frac{1}{T})$. (14)

Note that a factor $\frac{1}{T}$ has been incorporated in the σ_{1k} and π_{1k}, and $\frac{1}{T^2}$ in the ϵ''_{1k} and λ''_{1k}. These factors are, in fact, part of the affinities.

We comment briefly on the definition of heat flow.

The heat current w is the kinetic energy current density of the electrons, and therefore equal to the internal energy current density minus the potential energy current density,

$$w = u - \mu_e J. \tag{15}$$

We will from now on call it the absolute heat current density in contradistinction to

$$w^* = u - \mu J, \tag{16}$$

which, after Callen, we will call simply the heat current density. It follows that

$$w^* = u - (\mu_e + \mu_c)J = w - \mu_c J. \tag{17}$$

Our dynamical equations, rewritten in the condensed tensor notation

$$
\begin{aligned}
J &= \sigma E^* - \epsilon'' G \\
w^* &= -\pi'' E^* + \lambda'' G
\end{aligned}
\tag{18}
$$

will, therefore, using the electrostatic potential E and the absolute heat current density w, be written as:

$$
\begin{aligned}
J &= \sigma \left[E - \frac{1}{e} \nabla \mu_c \right] - \epsilon'' G \\
w - \mu_c J &= -\pi'' \left[E - \frac{1}{e} \nabla \mu_c \right] + \lambda'' G.
\end{aligned}
\tag{19}
$$

As will be shown in Chapter III, the experimental procedure was such that w* and E* appeared as the directly measurable quantities; for most of our derivations the more elegant system of equation (18) will, therefore, be used.

3. The Reciprocal Relations

As was shown above, the system of equations

$$J = \sigma E^* - \epsilon'' G$$
$$w^* = -\pi'' E^* + \lambda'' G \qquad (18)$$

is in the form suitable for the application of Onsager's theorem,[2] i.e. the elements of each tensor play the role of kinetic coefficients. The symmetry properties of these tensors combined with Onsager's theorem will yield an important relationship between the absolute thermoelectric tensor ϵ and the Peltier tensor π.

The Symmetry Properties

When symmetry properties are taken into consideration further relations between coefficients can be deduced. We will first remark that in order that the equations shall hold it is not necessary that the system be strictly isotropic, but only that there be isotropy in the 1-2 plane, with the 3-axis in the direction of the external magnetic field. In the case of single crystal, it is of interest to note that physical isotropy is guaranteed by the Onsager relations if the crystallographic symmetry is such that the 3-axis is a 3-, 4-, or 6-fold

---

[2] H. B. Callen, Phys. Rev. 73, 1349 (1948).

rotation axis, with the currents and forces being coplanar (in the 1-2 plane).[3]

We will restrict ourselves to this case. It can be shown that in the tensors, all terms related to the 3-axis vanish, and the problem reduces to a 2-dimensional problem, as fluxes and affinities parallel to the magnetic field vanish. The tensors will, from here on, be 2 by 2 tensors of the form

$$\begin{matrix} \epsilon'_{11} & \epsilon'_{12} \\ \epsilon'_{21} & \epsilon'_{22} \end{matrix} \text{ , etc.}$$

The assumed isotropy in the 1-2 plane gives immediately relations of the type

$$\begin{aligned} \epsilon'_{11} &= \epsilon'_{22} \\ \epsilon'_{12} &= -\epsilon'_{21} \end{aligned} \tag{20}$$

Now, considering the tensor elements in their functional dependence on the magnetic field, the following can be said: Suppose one reverses the magnetic field and then rotates the whole crystal around the 1-1 direction. As far as the relationship between the medium and the external magnetic field is concerned, the physical situation is identical to the original one. Taking again as a representative example the case of the ϵ' tensor we have, for the initial situation:

$$\begin{aligned} J_1 &= -\epsilon'_{11}(H)G_1 - \epsilon'_{12}(H)G_2 \\ J_2 &= -\epsilon'_{21}(H)G_1 - \epsilon'_{22}(H)G_2. \end{aligned}$$

for the final situation, the magnetic field and the affinities and fluxes along the 2-2 direction have changed sign, while the affinities

---

[3] L. Onsager, Phys. Rev. 37, 405 (1931); 38, 2265 (1931).

and fluxes along the 1-1 have not:

$$J_1 = -\epsilon''_{11}(-H)G_1 + \epsilon''_{12}(-H)G_2$$

$$-J_2 = -\epsilon''_{21}(-H)G_1 + \epsilon''_{22}(-H)G_2$$

The identification of these two systems of equations gives:

$$\begin{aligned} \epsilon''_{11}(-H) &= \epsilon''_{11}(H) \\ \epsilon''_{21}(-H) &= -\epsilon''_{21}(H) \end{aligned} \tag{21}$$

In general, therefore, all off-diagonal terms are odd functions of H, and all diagonal terms are even functions of H.

To apply Onsager's theorem consider again the equations in their developed 2-dimensional form:

$$\begin{aligned} J_1 &= \sigma_{11}E_1^* + \sigma_{12}E_2^* - \epsilon''_{11}G_1 - \epsilon''_{12}G_2 \\ J_2 &= \sigma_{21}E_1^* + \sigma_{22}E_2^* - \epsilon''_{21}G_1 - \epsilon''_{22}G_2 \\ w_1^* &= -\pi''_{11}E_1^* - \pi''_{12}E_2^* + \lambda''_{11}G_1 + \lambda''_{12}G_2 \\ w_2^* &= -\pi''_{21}E_1^* - \pi''_{22}E_2^* + \lambda''_{21}G_1 + \lambda''_{22}G_2 \end{aligned} \tag{22}$$

It is worthwhile stating fully now, the theorem in this special case:

Consider the linear effect of the first thermal affinity G_1/T^2 on the first electrical flux J_1. This will be equal to the effect of the first electrical affinity E_1^*/T on the first thermal flux w_1^*, measured in the reversed magnetic field. Thus,

$$T\epsilon''_{11}(H) = \pi''_{11}(-H)$$

but π''_{11} is an even function of the field: $\pi''_{11}(-H) = \pi''_{11}(H)$, Hence,

$$T\epsilon''_{11}(H) = \pi''_{11}(H) \tag{23}$$

Similarly consider the linear effect of the 2^d thermal affinity G_2/T^2 on the first electrical flux J_1. This will be equal to the

linear effect of the first electrical affinity E_2^*/T on the 2^d thermal flux w_2^*, measured in the reversed magnetic field. Thus,

$$T\epsilon''_{12}(H) = \pi''_{21}(-H)$$

but π''_{21} is an odd function of the magnetic field:

$$\pi''_{21}(-H) = -\pi''_{21}(H)$$

and from symmetry consideration,

$$\pi''_{21}(H) = -\pi''_{12}(H) \tag{24}$$

hence,

$$T\epsilon''_{12}(H) = \pi''_{12}(H) \tag{25}$$

or in tensor notation:

$$\pi'' = T\epsilon''. \tag{26}$$

In resume:

The problem is 2-dimensional.

Each tensor is a linear combination of the unit matrix with an antisymmetric matrix.

The Onsager relation apply under form:

$$\pi'' = T\epsilon''$$

The 2 x 2 matrices we have defined have the properties:

$$a_{11} = a_{jj}$$

$$a_{1j} = -a_{j1},\ j \neq 1.$$

In precise terms, they are a linear combination of an antisymmetric matrix with the unit matrix. We will, for brevity, call them "2 x 2 antisymmetric." One proves easily the following properties of these matrices:

1. Their sum and product are "2 x 2 antisymmetric."
2. Their reciprocal and the ratio of two such matrices are also "2 x 2 antisymmetric."

4. The Three Different Tensorial Representations

The system of equations we have used

$$\begin{aligned} j &= \sigma E^* - \epsilon' G \\ w^* &= -\pi E^* + \lambda' G \end{aligned} \tag{18}$$

implies the consideration of $G = -\nabla T$ and $E^* = -\frac{\nabla \mu}{e}$, as independent variables. This agrees with the theoretician's approach, who, in general, considers the electric field and the gradient of temperature as given and calculates the currents. Furthermore, one sees that the thermoelectric tensor ϵ' and Peltier tensor π' are, in analogy with the conductivities, directly dependent on the number of carriers.

Turning to the point of view of the experimentalist who prefers to speak in terms of resistivities, two approaches can be taken.

In the first one,[4,5] the electric current and the gradient of temperature are the independent variables, and one writes:

$$\begin{aligned} E^* &= \rho J + \epsilon G \\ w^* &= -\pi J + \lambda G \end{aligned} \tag{26}$$

This formulation has an important advantage in the study of the thermoelectric effect and the Peltier effect. In both these cases, one has to consider the junction of two different materials and the fact that at an isothermal junction, both the electric current I and the electrochemical potential μ are continuous. It follows that the terms corresponding to each side of the junction will appear as

---

[4] J. P. Jan, in Solid State Physics, Vol. 5, F. Seitz and D. Turnbull, editors, Academic Press, Inc., New York, 1957.

[5] See also P. Mazur and I. Prigogine, J. Phys. Radium 12, 616 (1951).

related simply by their difference. This will be shown in detail in Chapter III (Experimental Procedure).

The second approach corresponds to the experimental situation where one had direct control on the electric current and the heat current. This will correspond to the system of equations:

$$\begin{aligned} E^* &= \rho' J + \epsilon' w^* \\ G &= \pi' J + \lambda^{-1} w^* \end{aligned} \tag{27}$$

The independent variable being the currents, and the measured quantities being the electrostatic field and the gradient of temperature.

5. Relations Between the Different Tensors

The relations existing between the three thermoelectric tensors and the three Peltier tensors can be found as follows. Suppose $J = 0$; then from (26) $E^* = \epsilon G$ obtains, and from (18) $E^* = \epsilon'' \sigma^{-1} G$ obtains, hence,

$$\begin{aligned} \epsilon'' &= \sigma\epsilon. \\ \pi'' &= \sigma\pi \end{aligned} \tag{28}$$

Similarly taking $G = 0$, obtains. By the same mechanism, from (26) and (27),

$$\begin{aligned} \epsilon' &= \lambda^{-1}\epsilon \\ \pi' &= \lambda^{-1}\pi \end{aligned} \tag{29}$$

and consequently,

$$\begin{aligned} \epsilon'' &= \sigma\lambda\epsilon' \\ \pi'' &= \sigma\lambda\pi' \end{aligned} \tag{30}$$

Also relations will exist between ρ, σ, λ and other tensorial quantity

with $J = 0$ in (26) and (27), $\frac{1}{\lambda} = \lambda^{-1}$

with $G = 0$ in (18) and (26), $\rho = \frac{1}{\sigma} = \sigma^{-1}$

with $w^* = 0$ in (18) and (27), $\pi''\rho' = \pi'\lambda''$

with $w^* = 0$ in (26) and (27), $\rho' = \rho + \epsilon\pi\lambda^{-1}$

All these relations combined with the properties of "antisymmetric" tensors yield:

1. Any of the tensors used in (18), (26), and (27) are "antisymmetrical."

2. That the Onsager relation

$$T\epsilon'' = \pi''$$

extend simply through (28) to $T\epsilon = \pi$ (31)

and through (29) to $T\epsilon' = \pi''$

6. The Generalized Wiedemann-Franz Law

We have seen that the Onsager Theorem provides a general relation between the absolute thermoelectric power tensor and the Peltier tensor. It doesn't provide any relation between the thermal and electrical conductivity tensors. But the Wiedemann-Franz law is known to relate thermal and electrical conductivities:

$$\frac{\lambda}{\sigma} = LT \tag{32}$$

and from free electron theory, L should be a universal constant

$$L_n = \frac{\pi^2}{3}\left(\frac{k}{e}\right)^2 = 2.45 \times 10^{-8}\ \left(\frac{\text{volt}}{\text{deg}}\right)^2 \tag{33}$$

Kohler[6] has shown that the law should apply to a single crystal, for arbitrary orientation and magnitude of the magnetic field, provided the conduction electrons are scattered without change of energy. The law should be valid for all components of the conductivity tensors:

$$\lambda_{ik}(B) = L_n T \sigma_{ik}(B) \tag{34}$$

---

[6] M. Kohler, Ann. Physik 40, 601 (1941).

This relationship implies the equality of the Hall and Righi-Leduc angles, as the following shows:

We define

$$t_g\phi = \frac{\rho_{21}}{\rho_{11}} \tag{35}$$

and

$$t_g\phi' = + \frac{\lambda_{21}^{-1}}{\lambda_{11}^{-1}} \, . \tag{36}$$

The generalized law of Wiedemann-Franz

$$L_nT = \frac{\lambda_{1k}(B)}{\sigma_{1k}(B)} = \frac{\lambda_{11}}{\sigma_{11}} = \frac{\lambda_{21}}{\sigma_{21}} \tag{37}$$

would imply

$$\frac{\sigma_{21}}{\sigma_{11}} = \frac{\lambda_{21}}{\lambda_{11}} \tag{38}$$

but

$$\sigma_{21} = - \frac{\rho_{21}}{\rho_{11}^2 + \rho_{21}^2} \, , \; \lambda_{21} = - \frac{\lambda_{21}^{-1}}{(\lambda_{11}^{-1})^2 + (\lambda_{21}^{-1})^2} \tag{39}$$

and

$$\sigma_{11} = \frac{\rho_{11}}{\rho_{11}^2 + \rho_{21}^2} = \sigma_{22}, \; \lambda_{11} = + \frac{\lambda_{11}^{-1}}{(\lambda_{11}^{-1})^2 + (\lambda_{21}^{-1})^2} = \lambda_{22}$$

$$- \frac{\sigma_{21}}{\sigma_{11}} = \frac{\rho_{21}}{\rho_{11}} \quad \text{and} \quad - \frac{\lambda_{21}}{\lambda_{11}} = \frac{\lambda_{21}^{-1}}{\lambda_{11}^{-1}} \tag{40}$$

shows that (38) and (37) are equivalent to

$$t_g\phi = t_g\phi' \tag{41}$$

It is known that departures from the Wiedemann-Franz law occur both at intermediate temperatures and whenever the lattice thermal conductivity cannot be neglected.

The experimental determination of ρ_{21}, ρ_{11} in the galvanomagnetic case,* and of λ_{21}^{-1}, λ_{11}^{-1} in the thermomagnetic case, will allow us, therefore, to separate electron conductivity from lattice conductivity and consequently to check whether the Wiedemann-Franz law holds in the quantized situation of de Haas-van Alphen-type oscillatory phenomena. If the Wiedemann-Franz law holds, the relative change in thermal conductivity is equal to the relative change in electrical conductivity. This, as well as the dependence of the Lorenz number upon magnetic field predicted by the Sondheimer-Wilson theory, will be studied through our experimental results.

---

*These galvanomagnetic quantities have been initially measured by Dr. C. G. Bergeron and described in his dissertation. We made a new series of measurements of these quantities and found that they agreed very well with the period of oscillations.

CHAPTER II

EXPERIMENTAL APPARATUS

1. Basic Measuring Circuit, Magnet, and Helium Vacuum System

The circuit used for the measurement of the oscillatory potentials consisted of the following units: a Rubicon Microvolt Potentiometer (Rubicon Company, Philadelphia, Penn.); a Liston Becker dc breaker amplifier (Liston Becker Instrument Co., Inc., Stamford, Conn.) and a Brown recorder (Minneapolis Honeywell Co., Minneapolis, Minn.). These units have been already described by S. A. Ali[7] and C. G. Bergeron.[8] We will comment only on the features that were specifically important in our experiments.

The Rubicon Microvolt Potentiometer is especially devised to minimize any gradient of temperature across its inputs, its being encased in a heavy aluminum casing. This isothermal property plays an important role in the interpretation of the results concerning the thermoelectric power measurement, as will be seen further below. The potentiometer was used also as a bias voltage source in performing the potential measurements.

---

[7] S. A. Ali, Dissertation, Louisiana State University, 1958.

[8] C. G. Bergeron, Dissertation, Louisiana State University, 1959.

The electromagnet used was an iron core Weiss magnet with 8-inch pole pieces separated by a 1 5/8 inch airgap. It could be rotated 360° about a vertical axis and positioned within one-fourth of a degree. The magnet was calibrated by a nuclear resonance flux meter. Fig. 1 represents the magnetic field strength versus current. It can be seen that linearity in function of the current is good up to 33 amperes, with a slope of 1/2.97 kilogauss per ampere. The magnet control circuit has been described by Ali[9] and a schematic is given by him. The exciter coil of the dc generator in series with a set of 12 parallel 6AS7's. The exciter current through this circuit is controlled by an amplified "difference" voltage, appearing across a variable helipot and the magnet coils. When this "difference" voltage is not zero, the current through the exciter coil--6AS7 circuit adjusts itself in a direction to make the "difference" voltage approach zero. A continuous field sweep was achieved by driving the helipot with a small clock motor. The magnet current was monitored with a Rhodes voltmeter-potentiometer (Sensitive Research Instrument Corp., New York). It measured the voltage across a standard resistance (0.01 ohm) which was in series with the magnet.

To achieve a liquid helium bath temperature below 4.2°K, the vapor pressure of the bath was lowered by means of Kinney high capacity vacuum pump (Kinney Manufacturing Division, the New York Air Brake Co.,

---

[9]See Ref. 7.

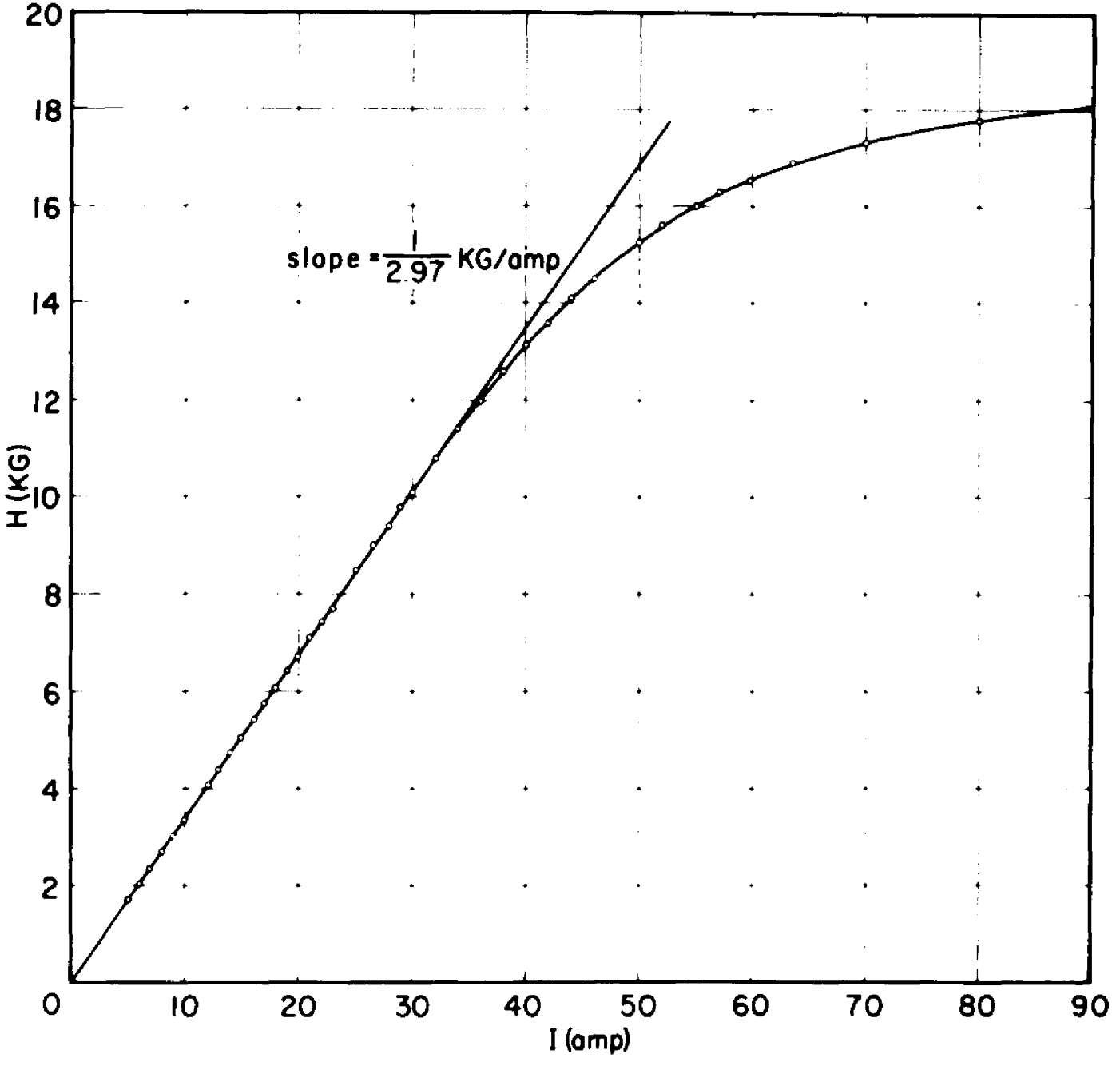

Fig. 1. Magnet Calibration Curve.

Boston, Mass.). The whole pumping set up described already by Bergeron,[10] is shown in detail in Fig. 2.

1-1. The Crystal

The sample was chemically cut from a single crystal of zinc grown by a modified Bridgman method. The sample dimensions were 26.58 x 8.1 x 0.345 mm. It was cut from the mother crystal in such a manner that, when placed vertically in the cryostat (i.e. the long length of the crystal being vertical) its hexagonal axis lay in the horizontal plane making an angle of 44° with the normal to the large face of the crystal. Its orientation was carefully determined by an X-ray diffraction study.

It will be noted here that the orientation of the hexagonal axis of the zinc crystal was not perpendicular to the plane of the sample. This difference with the ideal case of isotropy in the 1-2 plane, assumed in the introduction does not, however, entail troublesome consequences. The hexagonal axis was perpendicular to either the heat current or electric current direction. But it was at angle of $\theta = 44°$ with the direction of the transverse probes.

If d is the vector distance between the probes, the measured temperature difference is given by

$$T = - G \cdot d = -w_1(\lambda_{11}^{-1}d_1 + \lambda_{11}^{-2}d_2 + \lambda_{11}^{-3}d_3)$$

with $J_1 = J_2 = J_3 = 0$ and $w_2 = w_3 = 0$ (adiabatic condition) and where d_1, d_2, d_3 are the components of the probe distance along the current

---

[10] See ref. 8.

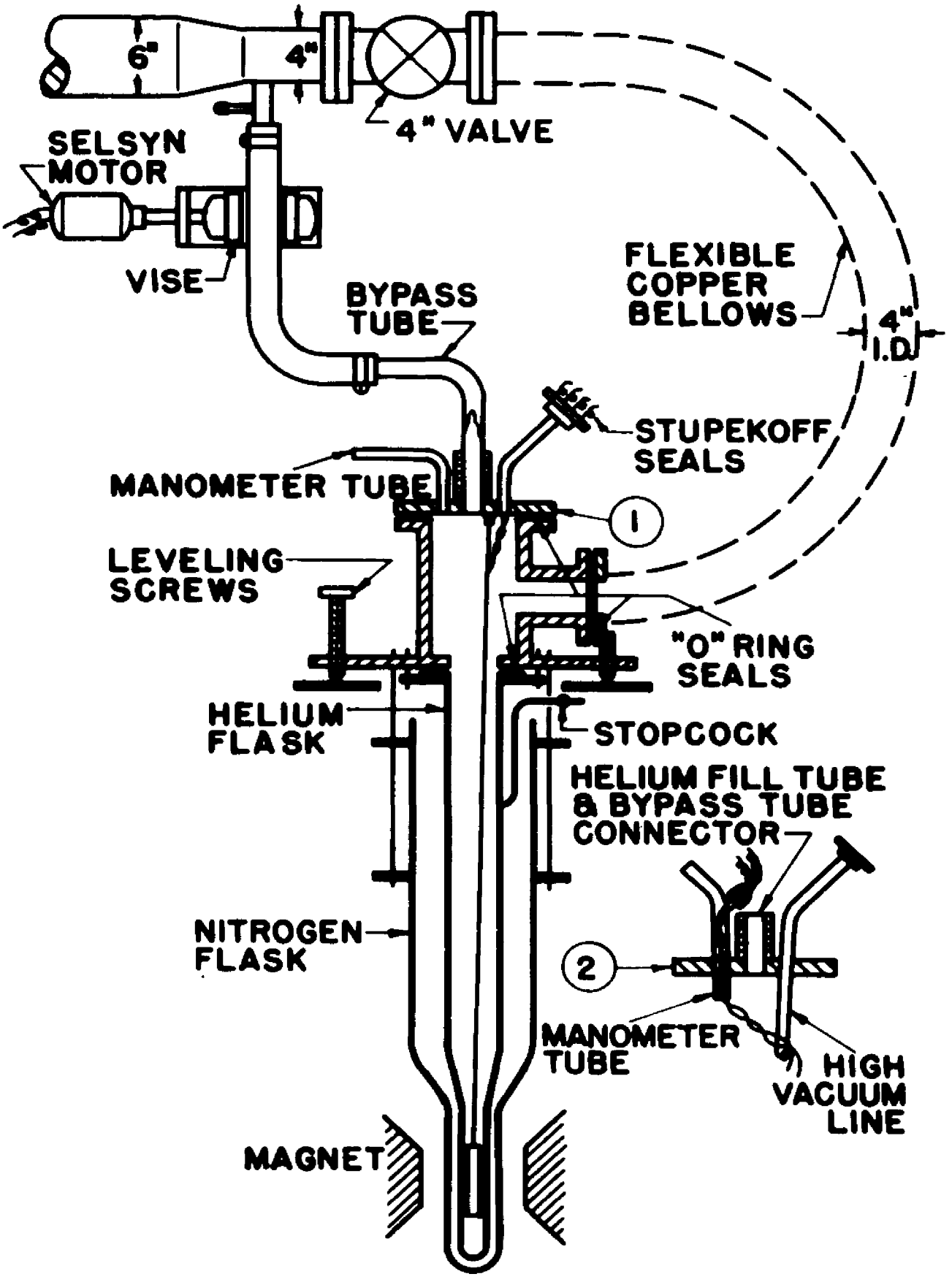

Fig. 2. Helium Dewar and Pumping System.

w_1, $(0x_1)$ mutually perpendicular to the current and the field $(0x_2)$, and parallel to the field $(0x_3)$ respectively. In the Righi-Leduc measurements the misalignment of the probes, d_1, introduces a thermal magnetoresistance effect. The effective probe separation for the Righi-Leduc effect is d_2 and d_3 is the probes separation along the magnetic field direction. In this case where the hexagonal axis is parallel to the field, but makes an angle θ with the normal to the large face of the crystal:

$$d_2 = d \cos\theta, \quad d_3 = d \sin\theta$$

$$\frac{\partial T}{\partial x_1} = - w_1 \lambda_{11}^{-1} d_1 \text{ and } \frac{\partial T}{\partial x_1}(H) = \frac{\partial T}{\partial x_1}(-H)$$

$$\frac{\partial T}{\partial x_2} = - w_1 \lambda_{21}^{-1} d_2 \text{ and } \frac{\partial T}{\partial x_2}(H) = - \frac{\partial T}{\partial x_2}(-H)$$

$$\frac{\partial T}{\partial x_3} = -w_1 \lambda_{31}^{-1} d_3 \text{ and } \frac{\partial T}{\partial x_3}(H) = - \frac{\partial T}{\partial x_3}(-H) \text{ or } 0$$

$\frac{\partial T}{\partial x_3} = 0$ when H is the hexagonal direction and the current is perpendicular to it. This is the experimental situation.

In case of misalignment of the field with the hexagonal axis

$$\frac{\partial T}{\partial x_3}(H) = \frac{\partial T}{\partial x_3}(-H),$$

i.e. λ_{31}^{-1} is even function of the field. Therefore, the experimental procedure gives:

$$\Delta T(H) - \Delta T(-H) = 2 \frac{\partial T}{\partial x_2}$$

and

$$\lambda_{21}^{-1} = - \left[\Delta T(H) - \Delta T(-H)\right] / 2 w_1 \, d \cos\theta.$$

Measurements were made for both H and -H and λ_{21}^{-1} was deduced from the above equation.

2. The Carbon Resistance Thermometers and Their Calibration Curves

The measurements of the Righi-Leduc and thermal magnetoresistance effects, and of the Peltier and Ettingshausen effects were primarily a measurement of small temperature differences.

The use of commercial radio-type resistors manufactured by the Allen-Bradley Company as thermometers is well-known since the original work of Clement and Quinnell.[11] These resistors exhibit a resistance which varies rapidly with temperature, particularly in the liquid helium range. Four useful features of these carbon resistors are their comparative insensitivity to magnetic fields and almost complete insensitivity to the value of the measuring current, apart from considerations of self-heating as well as their high sensitivity at sufficiently low temperature and their small heat capacity.

A group of 24 Allen-Bradley resistors was used, nominal value 50 ohm at room temperature, size 1/10 watt. A special run at liquid helium temperatures was made in order to select two pairs of "matched" resistors, i.e. with suitably identical R = f(T) characteristics. All 24 resistors were connected in series to a 6-volt battery through a commercial 1 Mohm resistance. This provided a stable current of 5.4 microamperes. Across each resistor a pair of copper leads was soldered thus allowing the measurement and comparison of their individual RI drop. A single measuring circuit composed of a Rhodes Potentiometer-voltmeter in series with a torsion galvanometer (used to supplement the

---

[11] J. R. Clement and E. H. Quinnell, Rev. Sci. Instr. 23, 213 (1952).

sensitivity of the potentiometer built-in galvanometer) was used. A first selection of six suitable pairs was made at 4.2°K on the basis of the individual resistance at that temperature. Then three other temperature points were covered namely 3.25°K, 2.10°K, and 1.26°K. At each of these temperatures, the torsion galvanometer was shorted out and the potentiometer was balanced for the two resistors of a pair. Their resistance was close enough so that the potentiometer reading was identical. Then the galvanometer would be introduced in the circuit and its deviation for each member of a pair, noted. In the final analysis of the results, the two pairs that had consistently shown equal resistances for the different temperatures were selected. It can be added that in spite of several cyclings between room temperature and liquid helium temperature, the pairs selected have consistently shown closely identical characteristic curves. (See Fig. 3).

3. Mounting of the Thermometers

The next problem was to insure good thermal contact between thermometers and crystal while keeping a very high electric insulation between them.

This was accomplished in the following way: A cylindrical sleeve of electrolytic copper was machined for each carbon resistor with an i.d. only slightly larger than the diameter of the resistor itself, i.e. a difference of about 6 mils. To each sleeve, a thermal lead made of copper wire No. 28 was soldered, all along the cylinder. Finally, electric insulation was insured by coating each resistor into a liquid plastic insulating compoung (Sherwin-Williams Co., Newark, N.J.) thinned into acetone. This proved to give a very thin but tough insulating jacket. The resistors were introduced in their sleeves

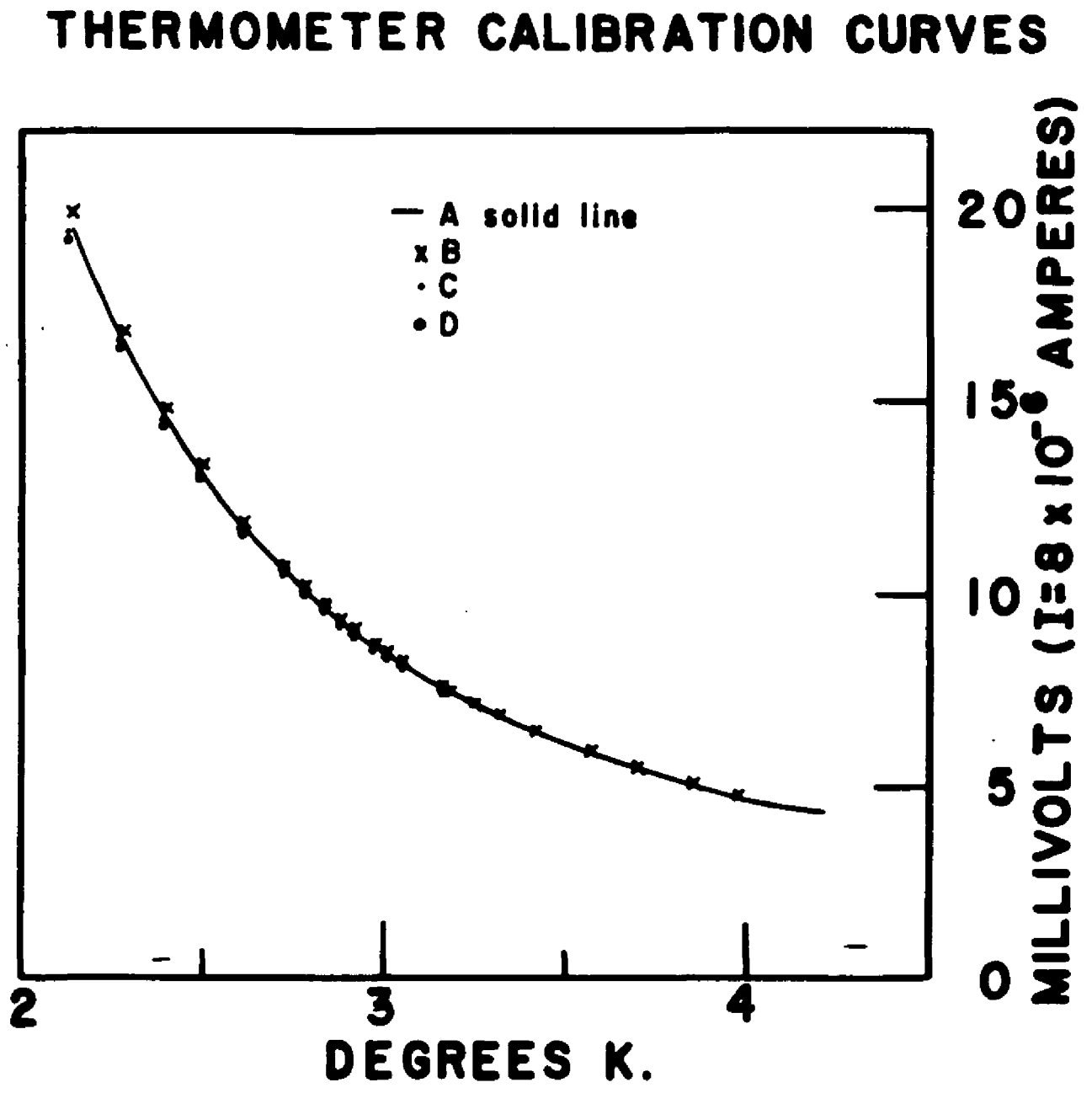

Fig. 3. Thermometers Calibration Curve.

while the compound was still liquid and left to dry. In practice, it appeared that every time the resistors were brought back at atmospheric pressure, their insulation from the thermal sleeve would deteriorate. But it would again become excellent when they were inside the high-vacuum calorimeter.

Next, to each resistor, two pairs of leads were soldered, one for the electric current circuit, the other for measurement of the difference of potential across the thermometer. These leads were made of "Advance" resistance wire No. 40, thus minimizing any instantaneous heat flow from the outside helium bath to the thermometers. Great care was taken to keep the resistances from heating up during the soldering of the leads, since any appreciable heating up would have changed their temperature characteristic thus spoiling the "matching" of a given pair. They were immerged almost totally in water, at the exception of the lead tip we were soldering to. Finally, the copper leads that were to serve as thermal junction between the sleeve of the thermometers and the crystal were soldered to the crystal.

4. <u>The Crystal Holder and Vacuum Calorimeter</u>

The vacuum calorimeter was a cylinder turned out of a solid piece of brass; it was secured to a brass lid by means of six brass screws, and a gold-wire ring provided a vacuum seal. The crystal to be investigated, had the form of a rectangular plate. It was mounted with its long dimension parallel to the axis of the brass vacuum jacket, with its upper part clamped to an electrolytic copper post extending up into the helium bath. The crystal was insulated electrically from the bar by means of cigarette paper and silicon vacuum grease.

The high purity copper post provided a good thermal contact with the helium bath by virtue of its flanged head, and it served as a heat sink for the heat current produced by a 40 gauge constantin wire heater wound around the lower end of the crystal. The heater was held in rigid thermal contact with the crystal by means of a solution of Dupont Duco Cement thinned in acetone. The position of the thermometers with respect to the crystal is shown in Fig. 5.

5. The Temperature Measuring Circuit

The thermometer circuit is shown in Fig. 6. It is composed of three parts described in the following.

The current circuit was in the form of a bridge: two arms of the bridge were constituted by the thermometers and the two other arms were constituted by a variable resistance box of high quality in series with a microammeter on one side, and by a standard resistance of 100 Kohms on the other side. Two commercial carbon resistances connected in parallel were in series with the batteries, giving a choice between the two values of 0.3 and 1 Megohm. The current used in the thermometers varied between 8 and 40 microamperes depending on the amplitude of the effect under measurement. Its value was constant at about 1%.

In the diagonal of the bridge was inserted the Rubicon Potentiometer. A procedure applied before each measurement consisted into balancing the two thermometers involved, so that, in the absence of the magnetic field, they would show a zero signal. To this effect, in the measurements of the transverse effects, the heater would first be connected. Then the resistance box was adjusted so that, when a change of the heat

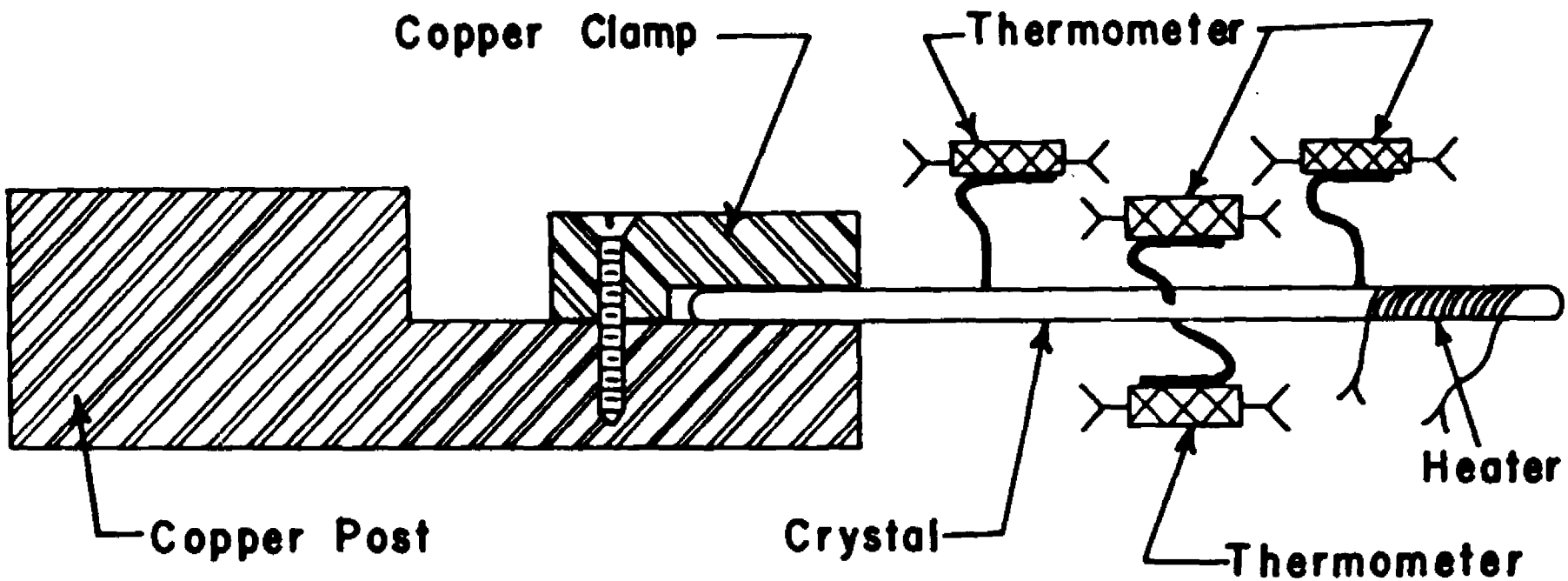

CRYSTAL HOLDER NUMBER I

Fig. 5

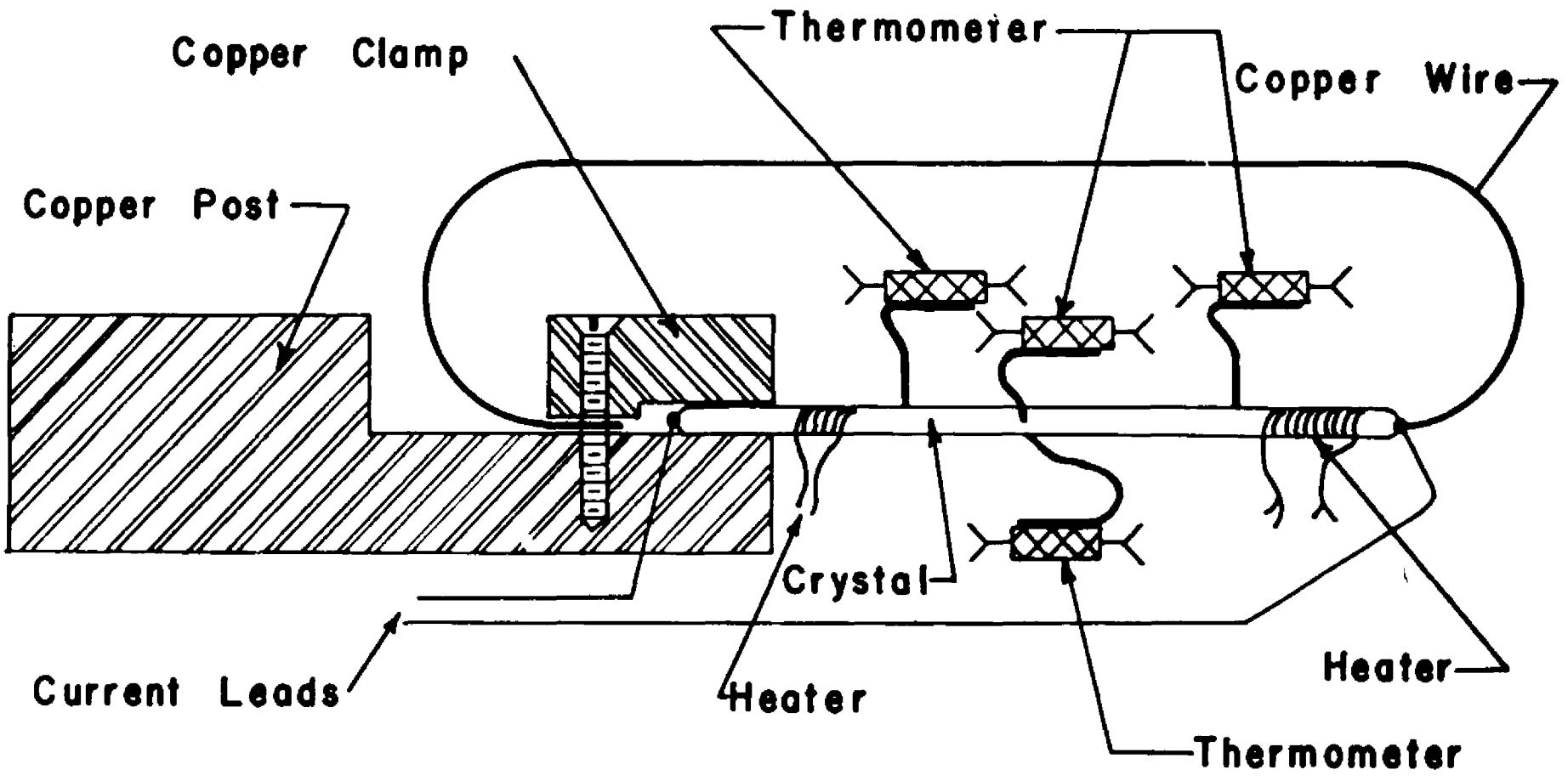

CRYSTAL HOLDER NUMBER 2

Fig. 5a

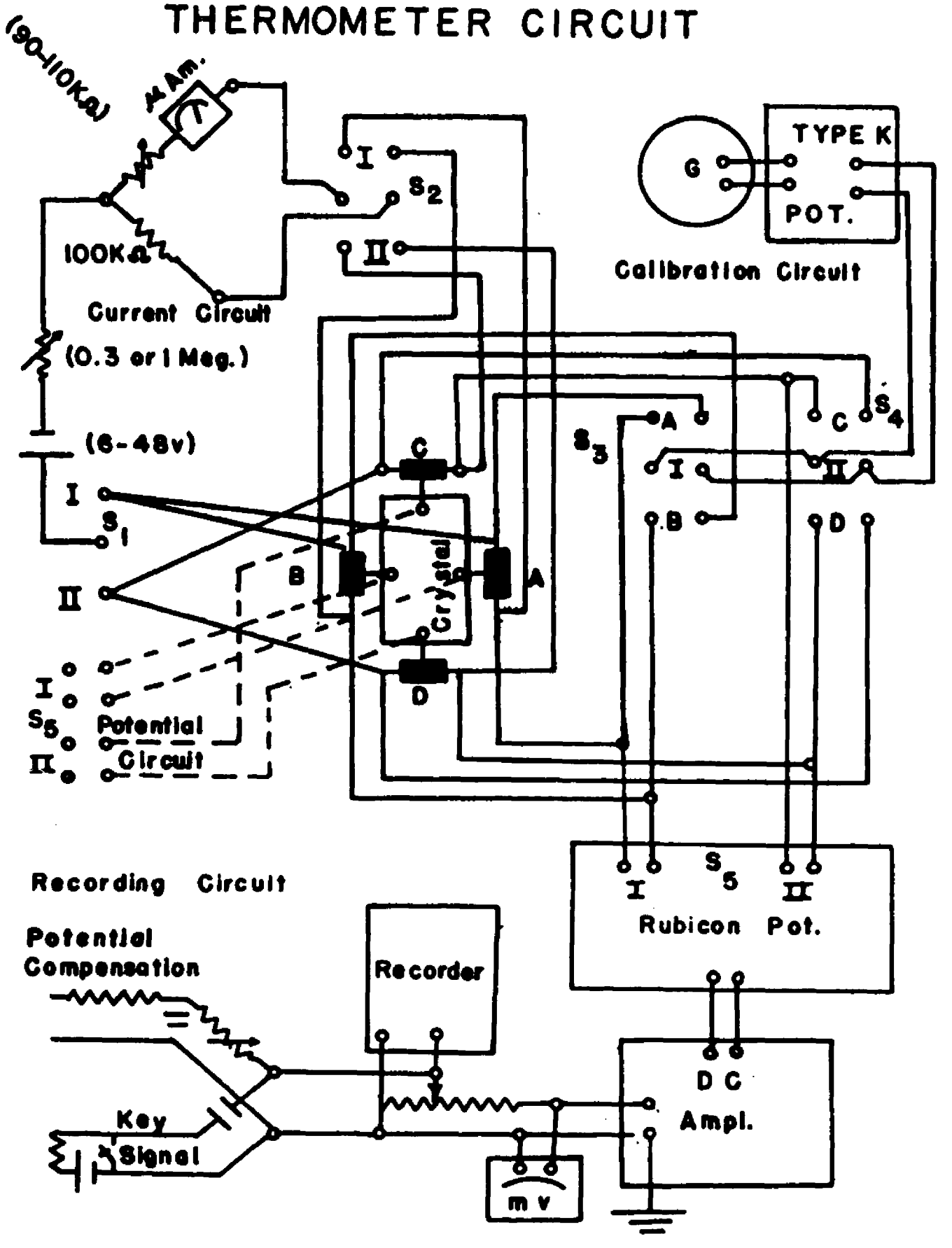

Fig. 6. The Thermometer Circuit.

current was produced, thus varying the temperature of the two thermometers equally, no signal would result. This insured that the two characteristic curves of the pair of thermometere were in coincidence, at the average temperature of the measurement.

In the case of longitudinal effects, the balancing was not as critical because only one end of the crystal and the corresponding thermometer were free to undergo a change in temperature. It was known that the thermometers had nearly identical characteristics, and the balancing consisted into adjusting the currents into the two arms of the bridge such that the voltages across each of the thermometers were equal.

The calibration circuit, i.e. the circuit allowing the measurement of the voltage across each thermometer separately, was constituted by a K2 potentiometer (Leeds and Northrup Co., Philadelphia, Penn.) and a galvanometer. This circuit was used to determine the characteristic $R = f(t)$ of each thermometer. This was done regularly during the decrease in temperature of the helium bath, at the start of each run. These characteristic curves were then used to interpret the voltage recorded V, in terms of differences of temperature, as will be explained in Chapter III, paragraph 5.

CHAPTER III

EXPERIMENTAL PROCEDURE AND OBSERVATIONS

1. Generalities

The general preparation of a run at liquid helium temperature has been described by Dr. C. G. Bergeron in his dissertation, and is now standard procedure in this laboratory. It will not be described again, mainly because the experimental procedure related to our experiments is rather involved and requires a thorough investigation. We shall, therefore, concentrate our attention on this investigation.

Since the measurements were concerned with variations of temperature gradients, the adiabaticity in the vacuum calorimeter was a sine qua noncondition. The utmost attention was, therefore, given to the monitoring of the high vacuum inside the calorimeter, by means of an ionization gauge. The vacuum was consistently better than 10^{-5} mm Hg, and usually stabilized, after the liquid helium transfer, at 2×10^{-6} mm Hg. After such a transfer, an immediate check was done on the continuity of the leads and the electrical insulation between the crystal on one hand and the carbon resistance thermometers and the heater winding on the other hand.

The orientation of the magnet so that the magnetic field direction would coincide with the hexagonal axis of the zinc crystal, was achieved before each run by locating the sharp relative minimum in the

magnetoresistance, either thermal or electrical, depending on the nature of the experiment.

Calibration Curves of the Thermometer

After each liquid helium transfer, the temperature of the bath would be cooled down by steps, through a controlled rate of pumping. For each step, the value of one or two thermometers of interest and the corresponding helium vapor pressure were recorded, after the vapor pressure had stabilized. This provided, for each experiment, a precise calibration curve of the thermometers involved, $V = f(T)$.

The comparison of the curves determined for different experiments shows that there is practically no hysteresis effect, i.e., the calibration curves of each thermometer stay identical to themselves in spite of the repeated cycling from room temperature to liquid helium temperatures.

In the last experimental run, all four thermometers were monitored simultaneously and the resulting points are shown in Fig. 3. It can be seen that their coincidence was very good.

2. <u>The Measurement of the Righi-Leduc and Thermal Magnetoresistance Effects</u>

A. Definition

The thermal conductivity of an isotropic homogeneous conductor in the presence of an external magnetic field (or as well, of a single crystal with sufficient symmetry in the plane perpendicular to the direction of the magnetic field) gives rise to two effects that were investigated.

The thermal magnetoresistance effect is characterized by the gradient of temperature $-G_1$ measured in the direction of a heat current w_1 when the external magnetic field is perpendicular to the current. It is a longitudinal effect in a transverse magnetic field.

The Righi-Leduc effect is characterized by the gradient of temperature $-G_2$ measured in the perpendicular direction to the heat current w_1, when the external magnetic field is perpendicular to both the current and the direction of the temperature gradient. It is a transverse effect in a transverse magnetic field.

One can say, by analogy with the Hall effect, that the Righi-Leduc effect is the phenomenon associated with the existence of a non-vanishing angle ϕ' between the gradient of temperature and the heat current lines.

The thermal conductivity in the absence of any electric current is described by the set of equations (in the 2-dimensional case):

$$\begin{aligned} w_1^* = w_1 &= \lambda_{11} G_1 - \lambda_{21} G_2 \\ w_2^* = w_2 &= \lambda_{21} G_1 + \lambda_{11} G_2 \\ J_1 = J_2 &= 0 \end{aligned} \tag{42}$$

The heat current and the gradient of temperature are in the 1-2 plane, while the magnetic field is in the 3-direction. One has

$$w^* = u - \frac{\mu}{e} J = w - \frac{\mu \zeta}{e} J = w$$

since $J = 0$; G is the negative temperature gradient, and one can define a Righi-Leduc angle ϕ' by the relation:

$$\tan \phi' = - \frac{\lambda_{21}}{\lambda_{11}} \quad . \tag{43}$$

In terms of thermal resistivities, one would write

$$\begin{aligned} G_1 &= \lambda_{11}^{-1} w_1 - \lambda_{21}^{-1} w_2 \\ G_2 &= \lambda_{21}^{-1} w_1 + \lambda_{11}^{-1} w_2 \end{aligned}$$

with the tensorial relations

$$\lambda_{11} = \frac{\lambda_{11}^{-1}}{(\lambda_{11}^{-1})^2+(\lambda_{21}^{-1})^2}\ ,\ \lambda_{21} = -\frac{\lambda_{21}^{-1}}{(\lambda_{11}^{-1})^2+(\lambda_{21}^{-1})^2} \tag{44}$$

and

$$\tan \varphi' = \frac{\lambda_{21}^{-1}}{\lambda_{11}^{-1}} \tag{45}$$

B. Experimental Procedure

The situation was that described in Chapter II, paragraph 4. The upper end of the zinc sample was clamped to the copper post which extended out into the helium bath. On the lower end, a heater wound with constantin wire No. 40, cotton insulated, brought a heat flow of about 1 milliwatt. The crystal was electrically insulated from both the heater and the copper post.

After the liquid helium transfer and a check on the vacuum, one of the transverse thermometers was monitored, identified as thermometer A, against the corresponding values of the helium vapor pressure. This provided a suitable calibration curve for the interpretation of the data. The field was then oriented along the hexagonal axis of the crystal by looking for the sharp relative minimum of thermal magneto-resistance. The heater was then turned on and the crystal average temperature, indicated by thermometer A, noted. Then one proceeded to record a sweep, with the magnetic field varying at a constant rate from 0 to 10 kilogauss. The magnet is then rotated by a 180 degrees, and another sweep taken with the magnetic field in the reverse direction. The difference of these two recordings eliminates any effect of misalignment of the transverse thermometers and provides twice the values of the

transverse gradient of temperature as a function of H. The thermal magnetoresistance measurement followed an identical procedure, but the field was not reversed. It is important to make the two following remarks:

1. It was estimated that the measurement of the residual thermal resistance $\lambda_{11}^{-1}(H = 0)$ was too imprecise to be taken into account. For, the rise of the crystal temperature and the corresponding correction to be made for the slight difference in the characteristic curves of the thermometers was of the same order, if not larger, than the effect itself. In the transverse case there evidently is no residual effect.

2. The zero of each recording was taken as being the trace of the recorder with heater turned on, in the absence of magnetic field. The measurement provided, therefore, the quantity:

$$\lambda_{11}^{-1}(H) - \lambda_{11}^{-1}(0) = \Delta\lambda_{11}^{-1}$$

The same remark applies to the electrical magnetoresistance measurements, $\rho_{11}(H) - \rho_{11}(0) = \Delta\rho_{11}$ except that in the electrical case the measurement of $\rho_{11}(0)$ does not present any difficulty and is made with relatively high precision.

Here are the principal details about these measurements:

Temperature of the helium bath: $1.37^{\circ}K$.

Temperature of the crystal ($H = 0$) with heater on (1 m watt): 2.00 K.

Heat current injected: 1 milliwatt or 35 milliwatt/cm^2.

C. Analysis of the Procedure

Let us state again the following definitions:

u = flow of internal energy.

w^* = T x flow of entropy = "heat current" = $u - \mu T$.

w = absolute heat current = $u - \mu cT$.

The experimental situation can be analytically described by (See Fig. 4): $w_2 = 0$, i.e. no transverse heat current, a condition that defines the adiabatic case. $J_1 = J_2 = 0$, i.e. no electric current either transverse or longitudinal. It follows that $w^* = w = u$ and, therefore,

$$w_i^* = w_i = \lambda_{ik} G_k \tag{46}$$

in tensor notation.

The consequence is that for the Righi-Leduc and the thermal magnetoresistance, the gradient of temperature one measures is:

$$G_i = \lambda_{ik}^{-1} w_k \tag{47}$$

where w_k is the absolute heat current injected in the crystal. In other words, the chemical part of the electrochemical potential has no bearing on these effects.

3. The Measurements of the Absolute Thermoelectric Power and the Nernst-Ettingshausen Effect

These measurements were done by Dr. C. J. Bergeron* and results are described in his dissertation. Though the same crystal was used, with the same type of holder, these effects were measured again in order to see whether the handling of the crystal and the soldering it

---

*C. J. Bergeron, Dissertation, Louisiana State University, 1959.

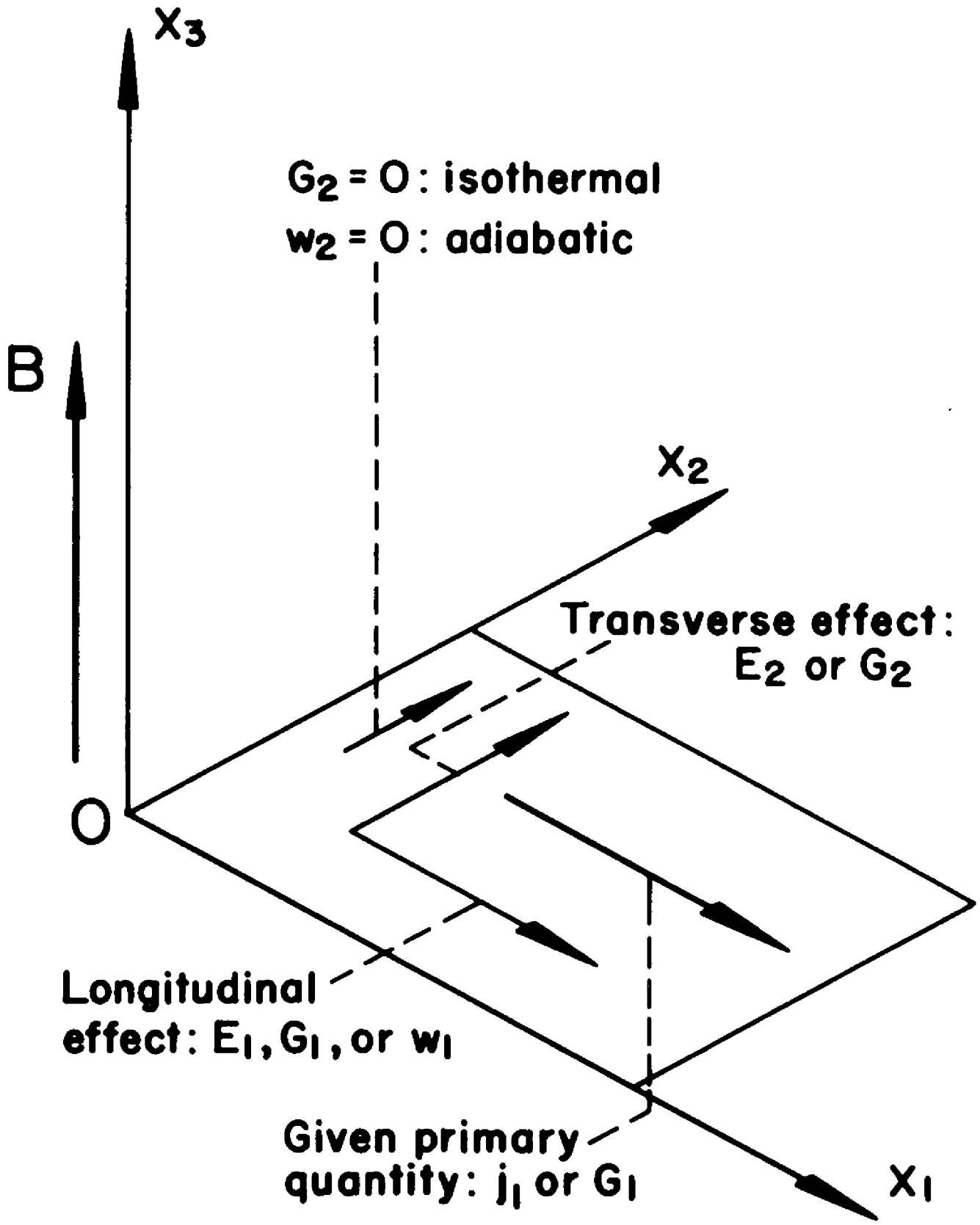

Fig. 4. Relative Orientations for Galvano- and Thermomagnetic Effects in a Transverse Magnetic Field.

underwent, had changed its characteristics. Our results coincided reasonably well with those of Dr. Bergeron, except for a slight reduction in the amplitude of the oscillations.

Analysis

An analysis that points to a fact overlooked in the previous work will now be given. The experimental situation is characterized by the conditions:

$$w_2 = 0, \; G_2 \neq 0$$
$$J_1 = J_2 = 0 \tag{48}$$

We have consequently again:

$$w^* = w = u = \lambda_{1k} G_k \tag{49}$$

These measurements were in fact a determination of the thermoelectric power of the Zn-Cu thermocouple formed by the zinc crystal and the copper leads. We will show that the ϵ tensor defined by

$$E^* = \rho J + \epsilon G \tag{50}$$

where

$$E^* = -\frac{1}{e}\nabla\mu, \; G = -\nabla T \tag{51}$$

is the difference of two terms, respectively related to the zinc sample and to the copper leads.

And idealized schematic of the experimental set up will be helpful. Junctions 1 and 2 are at temperatures T_1 and T_2 ($T_2 > T_1$) but three and four are at the same temperature T_p.

The kinetic equation (50), with J = 0 gives

$$E_1^* = \epsilon_{11} G_1 \tag{52}$$

where the problem is considered 1-dimensional, for simplicity. Noting that $E^* = \epsilon_{11} G_1$ and $G = -\nabla T$, one writes:

$$\begin{aligned} \mu_2 - \mu_1 &= -e \int_1^2 E_1^* dx = e \int_1^2 \epsilon_{11} G_1 dx = e \int_1^2 \epsilon_{11} dT \\ \mu_3 - \mu_2 &= -e \int_1^3 E_1^* dx = e \int_1^3 \epsilon_B dT \\ \mu_1 - \mu_4 &= e \int_4^1 \epsilon_B dT \end{aligned} \tag{53}$$

The elimination of μ_1 and μ_2, by adding the three relations gives:

$$\mu_3 - \mu_4 = e\left(\int_4^3 \epsilon_B dT + \int_2^1 \epsilon_B dT + \int_1^2 \epsilon_{11} dT \right) \tag{54}$$

But the important fact that the potentiometer is isothermal, i.e. no difference of temperature exists between 4 and 3 entails

$$\int_4^3 \epsilon_B dT = 0 \tag{55}$$

and most important, it entails also that $\frac{1}{e}(\mu_3 - \mu_4) = \frac{1}{e}(\mu_{e3} - \mu_{e4})$ as $\nabla \mu_c = 0$ across the isothermal potentiometer. $\frac{1}{e}(\mu_{e3} - \mu_{e4})$ is the difference of electrostatic potential, the potential which is measured by the potentiometer.

$$E^* = E \tag{56}$$

Since $\nabla \mu_c = 0$. This last point seems to have been overlooked in Bergeron's analysis. Therefore, the measured electrostatic potential, between 3 and 4 is:

$$V = -\frac{1}{e}(\mu_3 - \mu_4) = \int_1^2 (\epsilon_B - \epsilon_{11})dT = (\epsilon_B - \epsilon_{11})\,\Delta T \tag{57}$$

since the difference of temperature involved is very small. Now, since the diameter of the copper leads was very small (No. 33) any transverse effect in the leads due to the external magnetic field was negligeable. Therefore, going back to the 2-dimensional case we can consider a thermoelectric tensor for copper of the form:

$$\epsilon_B = \begin{vmatrix} \epsilon_B & 0 \\ 0 & \epsilon_B \end{vmatrix} \tag{58}$$

One has, therefore, in tensor notation:

$$E = (\epsilon - \epsilon_B)G \tag{59}$$

with the important relation

$$E = E^* \tag{60}$$

guaranteed by the isothermal nature of the potentiometer. To write (59) in developed form, we must take account of $G_2 \neq 0$. Hence,

$$\begin{aligned} E_1 = E_1^* &= (\epsilon_{11} - \epsilon_B)G_1 + \epsilon_{12}G_2 \\ E_2 = E_2^* &= \epsilon_{21}G_1 + (\epsilon_{11} - \epsilon_B)G_2 \end{aligned} \tag{61}$$

Relation of the Elements of Tensor ϵ with the Measured Quantities

The independent experimental parameter was the absolute heat current w_1, and the measurements determined the quantities

$$\epsilon'_{11} = \frac{E_1}{w_1}\ ,\ \epsilon'_{21} = \frac{E_2^*}{w_1} \tag{62}$$

Substituting $G_i = \lambda_{ij}^{-1} w_i$ in (61) it becomes:

$$\begin{aligned} \epsilon'_{11} &= (\epsilon_{11} - \epsilon_B)\lambda_{11}^{-1} + \epsilon_{21}\lambda_{12}^{-1} \\ \epsilon'_{21} &= \epsilon_{21}\lambda_{11}^{-1} + (\epsilon_{11} - \epsilon_B)\lambda_{12}^{-1} \end{aligned} \tag{63}$$

where we used the symmetry relation $\epsilon_{11} = \epsilon_{22}$. This can be written in tensor form

$$\epsilon' = \lambda^{-1}(\epsilon - \epsilon_B). \tag{64}$$

This describes accurately the effect of the presence of the copper leads.

It is worth pointing out that the use of the ϵ tensor enables us to introduce the effect of copper as a simple additive term to the diagonal elements of the ϵ tensor.

Relation of the Elements of Tensor ϵ'' with the Measured Quantities

If one rewrites the dynamical equations with the condition $J = 0$, one has in tensor form:

$$\begin{aligned} E^* &= \epsilon G \\ J &= \sigma E^* - \epsilon'' G \end{aligned} \tag{65}$$

the second of equations (65) yields:

$$\epsilon'' = \sigma e. \tag{66}$$

But since $$\epsilon' = \lambda^{-1}(\epsilon - \epsilon_B) \tag{67}$$

or $$\epsilon = \lambda\epsilon' + \epsilon_B$$

It follows from (66)

$$\epsilon'' = \sigma\,\lambda\epsilon' + \sigma\epsilon_B \tag{68}$$

The complete developed form will be given, since it was used in the calculations of the elements of the ϵ'' tensor:

$$\begin{aligned}\epsilon''_{11} &= \epsilon'_{11}(\sigma_{11}\lambda_{11} - \sigma_{21}\lambda_{21}) - \epsilon'_{21}(\sigma_{11}\lambda_{21} + \sigma_{21}\lambda_{11}) + \sigma_{11}\epsilon_B \\ \epsilon''_{21} &= \epsilon'_{21}(\sigma_{11}\lambda_{11} - \sigma_{21}\lambda_{21}) + \epsilon'_{11}(\sigma_{11}\lambda_{21} + \sigma_{21}\lambda_{11}) + \sigma_{21}\epsilon_B\end{aligned} \tag{69}$$

factor out $\sigma_{11}\lambda_{11}$ and use $\tan\phi = -\frac{\sigma_{21}}{\sigma_{11}}$, $\tan\phi' = -\frac{\lambda_{21}}{\lambda_{11}}$. (70)

If one now makes the assumption $\tan\phi = \tan\phi'$, which was proved to be equivalent to the validity of the generalized Wiedemann-Franz law, the expression simplifies into:

$$\begin{aligned}\epsilon''_{11}/\sigma_{11}\lambda_{11} &= \epsilon'_{11}(1 - \tan^2\phi) + \epsilon'_{21}\cdot 2\tan\phi + \epsilon_B/\lambda_{11} \\ \epsilon''_{21}/\sigma_{11}\lambda_{11} &= \epsilon'_{21}(1 - \tan^2\phi) - \epsilon'_{11}\cdot 2\tan\phi + \frac{\sigma_{21}}{\sigma_{11}}\frac{\epsilon_B}{\lambda_{11}}\end{aligned} \tag{71}$$

hence, dividing by $1 - \tan^2\phi = 1 - \tan\phi\tan\phi' = 1 - \frac{\sigma_{21}}{\sigma_{11}}\frac{\lambda_{21}}{\lambda_{11}}$

$$\begin{aligned}\epsilon''_{11} &= (\sigma_{11}\lambda_{11} - \sigma_{21}\lambda_{21})(\epsilon'_{11} + \epsilon'_{21}\tan^2\phi) + \sigma_{11}\epsilon_B \\ \epsilon''_{21} &= (\sigma_{11}\lambda_{11} - \sigma_{21}\lambda_{21})(\epsilon'_{21} - \epsilon'_{11}\tan^2\phi) + \sigma_{21}\epsilon_B\,.\end{aligned} \tag{72}$$

The quantities $\epsilon''_{21\ \text{calc.}}$ and $\epsilon''_{11\ \text{calc.}}$, that were computed and plotted are:

$$\begin{aligned}\epsilon''_{11\ \text{calc.}} &= (\sigma_{11}\lambda_{11} - \sigma_{21}\lambda_{21})(\epsilon'_{11} + \epsilon'_{21}\tan^2\phi) \\ \epsilon''_{21\ \text{calc.}} &= (\sigma_{11}\lambda_{11} - \sigma_{21}\lambda_{21})(\epsilon'_{21} - \epsilon'_{11}\tan^2\phi)\end{aligned} \tag{73}$$

they represent therefore:

$$\begin{aligned}\epsilon''_{11\ \text{calc.}} &= \epsilon''_{11} - \sigma_{11}\epsilon_B \\ \epsilon''_{21\ \text{calc.}} &= \epsilon''_{21} - \sigma_{21}\epsilon_B\end{aligned} \tag{74}$$

and contain implicitly a term proportional to ϵ_B.

4. The Measurement of the Peltier and Ettingshausen Effects

A. Definition of the Peltier effect and Ettingshausen effect.

The Peltier effect refers to the evolution of heat accompanying the flow of an electric current across an isothermal junction of two materials A and B. The total energy current U will be discontinuous across the junction, and the energy difference appears as "Peltier heat" at the junction. In the experimental set up, the junction is between a copper wire and a zinc crystal with widely different cross sections. We will accordingly speak of total currents. One has

$$U = W^* + \frac{\mu}{e} I, \text{ where } U \text{ and } I \text{ stand for the} \tag{75}$$

total currents and since both the electrochemical potential for electron μ and the electric current I are continuous across the junction it follows that the discontinuity in U is equal to the discontinuity in W^*.

$$U_A - U_B = W_A^* - W_B^* \tag{76}$$

since this occurs under isothermal condition the heat which evolves at the junction is

$$\Delta Q = T\Delta S = (W_A^* - W_B^*) \times \text{time}. \tag{77}$$

Because of the isothermal condition $G = 0$, the dynamical equations give in either conductor

$$W^* = -\pi'' E^* \tag{78}$$

In the one dimensional case that we are analyzing, the Peltier coefficient π_{AB} is defined as the heat that must be supplied to the junction when unit electric current passes from conductor A to conductor B. Thus,

$$\pi_{AB} = \frac{W_B^* - W_A^*}{I} = \frac{W_B^*}{J_B} - \frac{W_A^*}{J_A} = -\pi_B + \pi_A \qquad (79)$$

This definition can be extended to the case of homogeneous isotropic medium. The Peltier effect would characterize the heat flow accompanying an electric current and the Peltier coefficient would measure the gradient of temperature created per unit electric current.[12]

Ettingshausen effect: In the presence of a magnetic field, perpendicular to the electric current, the Ettingshausen coefficient measures the gradient of temperature per unit electric current, measured perpendicularly to both current and magnetic field.

B. The Experimental Procedure

In the experimental set up, the zinc crystal was connected at each end with the current leads (See Fig. 7). Thus, one must take into account the fact that one had two junctions Cu-Zn and Zn-Cu respectively. The junction at the extremity of the crystal that was in contact with the helium bath can be considered as isothermal. The quantities that were measured were the differences of temperature respectively between the two junctions, in the direction of the current and transverse to the current, as a function of the magnetic field strength for a constant electric current. We shall show in the analysis the relationship of the measured quantities to the Peltier and Ettingshausen coefficients.

The first try at the measurement of the Ettingshausen effect was done with the crystal mounted as described in Chapter II, i.e. with

---

[12] J. P. Jan, op. cit.

CIRCUIT FOR
CRYSTAL CURRENT
HEATER CURRENT
COMPENSATING HEATER CURRENT

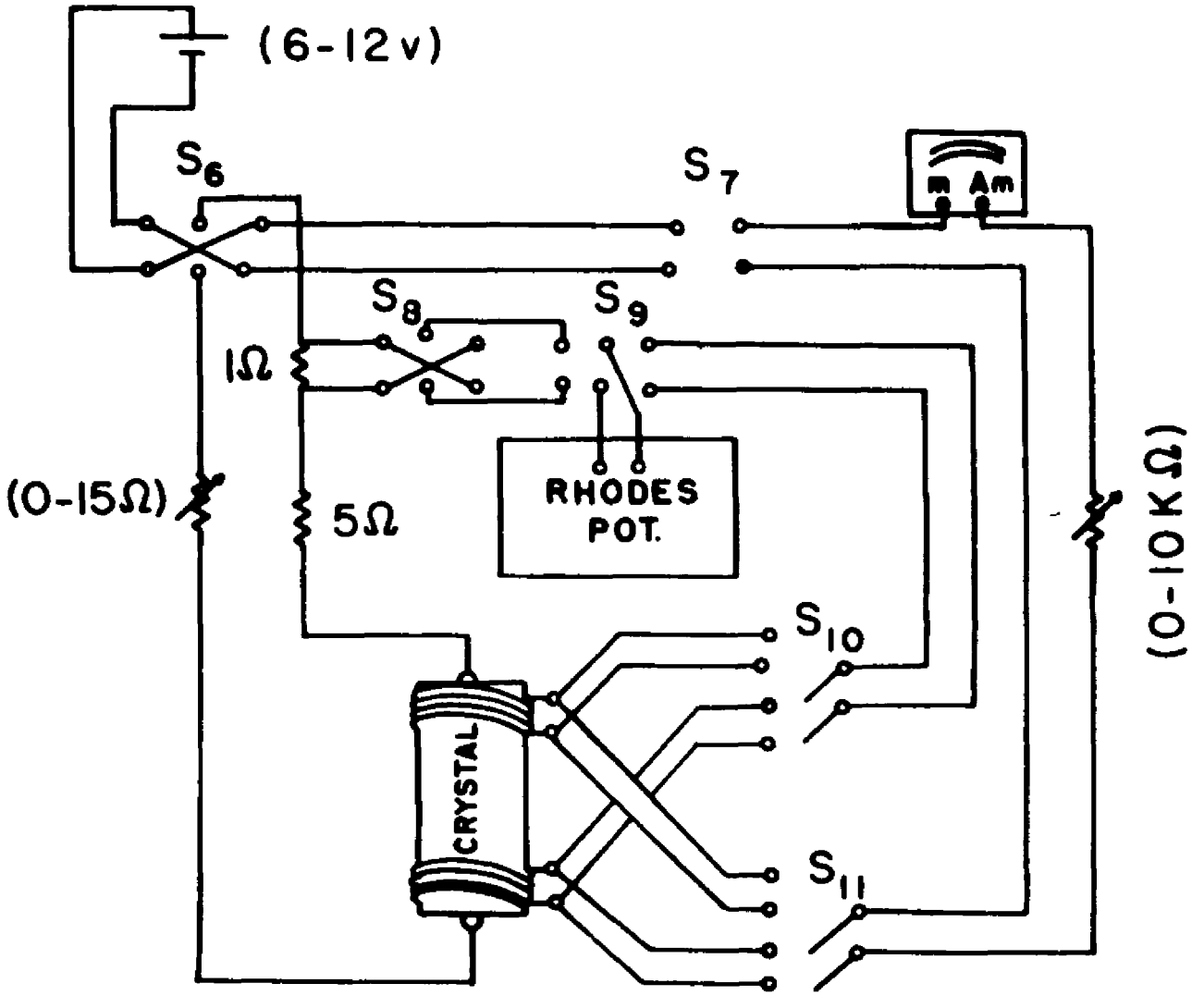

Fig. 7. Circuit for Crystal Current and Heaters Current.

one end in thermal contact with the helium bath, through an electrolytic copper post, the other end being thermally insulated. The measurement showed a large Righi-Leduc effect, indicating the flow of a rather large heat current along the crystal. The origin of this heat current was attributed to two simultaneous phenomena.

The first was obviously the creation of a large amount of Joule's heat, mainly in the small cross section copper leads. This produced a heat current flowing towards the heat sink provided by the copper post. This flow was creating not only a Righi-Leduc transverse gradient of temperature, but a longitudinal one, as well, due to the thermal magneotresistance effect.

The second was the evolution of a Thomson heat as the electric current traversed the longitudinal gradient of temperature. Under these conditions, the presence of large Righi-Leduc and magnetoresistance effects made impossible any measurement of the Peltier and Ettingshausen effects, since these are much smaller in absolute value.

A first try at minimizing the heat current was made, by winding a few turns of resistance wire on the clamped extremity of the crystal, to be used as auxiliary heater. The idea was to raise the temperature of that end so as to minimize the temperature gradient across the length of the crystal. This reduced effectively the heat current and the difference of two recordings with opposite values of the electric current showed a pure oscillatory effect that we tentatively identified with the Ettingshausen effect. But the precision was very poor and a more efficient way of minimizing the Joule heat current had to be found.

To this effect, a thermal junction was effected from the previously thermally insulated end of the crystal to the heat sink (copper post). We used a heavy copper wire (No. 22) soldered at one end to the extremity of the current lead where we suspected most of the Joule heat to originate, and clamped the other to the copper post. This arrangement proved very effective. Hence, a slight heat current injected at the principal heater proved to minimize any temperature gradient down to a negligeable amount. The heater was adjusted by trying to reduce the thermal magnetoresistance effect to a negligeable value, with a magnetic field of about 6.5 kilogauss present. The conditions in the final (and successful) run were the following:

For Ettingshausen Effect

Average temperature of helium bath: 1.49°K.

Electric current through crystal: 670 milliamperes.

Amount of heat injected (to neutralize the temperature gradient created by Joule heat): $\cong$ 0.6 milliwatt.

Average temperature of crystal: 2.98°K.

For Peltier Effect

Average temperature of helium bath: 1.82°K.

Electric current through crystal: 669 milliamperes.

Amount of heat injected: $\cong$ 0.36 milliwatts.

Average temperature of crystal: 2.90°K.

C. Analysis of the Experimental Procedure.

The basic experimental set up guaranteed the following conditions:

No transverse current flow $J_2 = 0$, and as a consequence $w_2^* = w_2 = u_2$.

No transverse heat flow $w_2 = w_2^* = 0$.

One end of the crystal, and the corresponding junction in contact with a heat reservoir, i.e. the helium bath.

The basic kinetic equations are, therefore,

$$\begin{aligned} w_1^* &= -\pi_{11} J_1 + \lambda_{11} G_1 + \lambda_{12} G_2 \\ 0 &= -\pi_{21} J_1 + \lambda_{21} G_1 + \lambda_{11} G_2 \end{aligned} \tag{80}$$

Our experimental procedure was to add the following feature:

1. The gradient of temperature created by the Joule's heat was minimized to a negligeable value as described in the procedure. The inherent Thomson effect which corresponds to this Joule's gradient of temperature was by the same way minimized.

2. The inherent Thomson effect that exists simultaneously with the Peltier gradient of temperature, was eliminated by taking two different sweeps with electric current +I and -I respectively, and substracting the two curves. It should be pointed out that this operation eliminates also any Righi-Leduc and magnetoresistance effects associated with a residual fraction of the Joule's heat current. This will be justified as follows. Consider the following schematic diagram:

It will be shown first that the Peltier effect is equivalent to the flow of a Peltier heat current in the sample. For, if the whole sample and the junctions are kept isothermal, an amount of heat equal to the Peltier heat will evolve from one junction to the reservoir while the same amount of heat is taken from a reservoir to the other junction. This is equivalent to the flow of heat

$$W_B - W_A = (\pi_A - \pi_B)I \tag{81}$$

Now suppose one of the junctions is not isothermal, as is the case in the experiment and the condition of the sample is adiabatic. A difference of temperature ΔT will be set up by the Peltier heat flow. The Thomson effect is proportional to both the current and the difference of temperature ΔT. When the current is reversed, the flow of Peltier heat reverses and the difference of temperature becomes $-\Delta T$. Therefore, the Thomson effect proportional to the product $J \times \Delta T = (-J) \times (-\Delta T)$ is <u>unchanged</u>, and is eliminated when the difference of the +I recording and -I recording is taken. The gradient of temperature associated with any residual Joule's heat flow will obviously remain unchanged when the electric current is reversed an the associated Thomson effect will not vanish in the difference, but will be negligible.

This being established, one has in the longitudinal direction calling A and B the respective cross sections for the zinc sample,

$$W_A^* \simeq -\pi_{11} I_1 + (\lambda_{11} G_1 - \lambda_{21} G_2)A \tag{82}$$

and for the copper leads,

$$W_B = -\pi_B I_1 \tag{83}$$

where we neglect all terms of the form $\lambda_B GB$ because of the smallness of the copper leads cross section.

The system of kinetic equations is, therefore,

$$W_A^* - W_B^* = -(\pi_{11} - \pi_B)I_1 + (\lambda_{11}G_1 - \lambda_{21}G_2)A \qquad (84)$$
$$0 = -\pi_{21}I_1 + (\lambda_{21}G_1 + \lambda_{11}G_2)A$$

and the continuity of the electrochemical potential at the junctions gives,

$$W_A^* = W_B^* = W_A - W_B \qquad (85)$$

It will now be shown that $W_A - W_B$ was negligible. The thermal resistances joining the ends of the crystal to the sink (copper post) were large as compared to that of the crystal itself. It was estimated that they were in the ratio of 1000 to 7. If this is compared to an equivalent electrical circuit, the crystal with the gradient of temperature along it, is equivalent to a cell, and its terminals are grounded through two large resistances. The external current is, therefore, small and the difference of potential measured across the cell will be close from the emf value. Similarly, the temperature difference measured across the sample will be close from the Peltier ΔT and the outside flow of heat current can be considered negligible. Therefore,

$$\begin{aligned} 0 &= -(\pi_{11} - \pi_B)I_1 + (\lambda_{11}G_1 - \lambda_{21}G_2)A \\ 0 &= -\pi_{21}I_1 + (\lambda_{21}G_1 + \lambda_{11}G_2)A \,. \end{aligned} \qquad (86)$$

Defining a tensor

$$\pi_B = \begin{vmatrix} \pi_B & 0 \\ 0 & \pi_B \end{vmatrix} \qquad (87)$$

this can be written tensorially, reverting to the density of current:

$$0 = (\pi - \pi_B)J + \lambda G \qquad (88)$$

or

$$G = \lambda^{-1}(\pi - \pi_B)J \,. \qquad (89)$$

The quantity determined experimentally being π', defined by

$$G = \pi' J \tag{90}$$

It follows that the relation between π and π', is:

$$\pi' = \lambda^{-1}(\pi - \pi_B) \tag{91}$$

or
$$\pi = \lambda\pi' + \pi_B \tag{92}$$

or developed form:

$$\begin{aligned} \pi'_{11} &= (\pi_{11} - \pi_B)\lambda_{11}^{-1} - \pi_{21}\lambda_{21}^{-1} \\ \pi'_{21} &= \pi_{21}\lambda_{11}^{-1} + (\pi_{11} - \pi_B)\lambda_{21}^{-1} \end{aligned} \tag{93}$$

This means that if one calculates π directly from the experimental π', by writing $\pi = \lambda\pi'$, one gets in reality

$$\begin{aligned} \pi_{11\text{calc.}} &= \pi_{11} - \pi_B \\ \pi_{21\text{calc.}} &= \pi_{21} \cdot \end{aligned} \tag{94}$$

Do the Onsager relations still apply to the experimental quantities π'_{11} and π'_{21} in spite of the introduction of a term related to the copper leads? Yes. For one has for zinc (reciprocal relations),

$$\pi = T\epsilon \tag{95}$$

and for copper

$$\pi_B = T\epsilon_B \tag{96}$$

(Copper leads from the same make have been used in both classes of experiments.), hence,

$$\pi - \pi_B = T(\epsilon - \epsilon_B) \tag{97}$$

but it was shown that

$$\begin{aligned} \pi' &= (\pi - \pi_B)\lambda^{-1} \\ \epsilon' &= (\epsilon - \epsilon_B)\lambda^{-1} \end{aligned} \tag{98}$$

therefore, one still has

$$\pi' = T\epsilon'. \tag{99}$$

Notice here, again, that the π notation in analogy to the ϵ notation has the advantage of introducing the effect of copper as a simple additive term.

Note: It was assumed that π_B contains no diagonal terms. That these terms are negligible can be seen from the fact that the thermometer are attached to the crystal at points that are far from the Cu-Zn junction, and, therefore, any end effect due to these off-diagonal terms will be negligible.

The relationship between π'' and π' is again obtained by the use of the general result $\pi'' = \sigma\pi$. Since π was determined in the experimental set up as being

$$\pi = \lambda\pi' + \pi_B$$

one has

$$\pi'' = \sigma\lambda\pi' + \sigma\pi_B. \qquad (100)$$

CHAPTER IV

EXPERIMENTAL RESULTS AND THEIR INTERPRETATION

The basic aim of this work was to seek an answer to the following questions.

Whether the temperature gradients associated with thermomagnetic and galvanomagnetic effects exhibit de Haas-van Alphen-type oscillations.

Whether the Wiedemann-Franz law holds for transverse as well as longitudinal* phenomena, in a transverse magnetic field; and the study of the related Lorenz ratio as a function of the magnetic field strength.

Whether Onsager's reciprocal relations hold under the extreme conditions of very low temperatures and quantum behavior (de Haas-van Alphen-type oscillations). In this respect, it is worth pointing out that the Onsager theorem is derived from first principles and is model-independent.

Tentatively, a comparison with some theoretical models will also be attempted.

1. The Righi-Leduc and Thermal Magnetoresistance Coefficients in Zinc

Note: In this chapter, for the sake of simplicity, the letter K will be used to designate thermal resistivity. This replaces the former notation λ^{-1}.

---

*The longitudinal phenomena having been already investigated by P. B. Alers, Phys. Rev. 101, 41 (1956).

1-1. The Righi-Leduc Resistivity K_{21}. The Righi-Leduc resistivity, i.e., the transverse thermal resistivity in a transverse magnetic field is characterized by the coefficient $K_{21} = G_2/w_1$ and its experimental behavior is plotted in Fig. 8. The average temperature of the crystal was 1.98°K.

In the same figure, results of the Hall effect measurements characterized by the coefficient $\rho_{21} = \frac{E_2^*}{J_1}$ have been represented. The crystal was in contact with the He II bath at 2°K, i.e. the Hall measurement was made under isothermal conditions. The two scales used in Fig. 8 were adjusted in a ratio equal to $L_n T$, where L_n is the free-electron value of the Lorenz ratio to facilitate the comparison on the basis of the Wiedemann-Franz law.

De Haas-van Alphen-type oscillations were found in the Righi-Leduc effect, superimposed on a smooth variation. The Righi-Leduc coefficient is positive for $H < 5580$ gauss and negative for larger values of the field. The oscillations in the two effects are closely in phase and the period as measured already by Bergeron is $P = 6.14 \times 10^{-5}$ gauss^{-1}.

Other measurements were taken at higher temperatures, namely at 4.2°K and 3.16°K. The sensitivity of the thermometers was poor at these temperatures. The results, as compared with those at 2°K, indicated qualitatively that the thermal resistivity varied as 1/T. Since previous measurements in this laboratory had shown that the electrical resistivity was independent of the temperature in this range, this agrees with what one would expect from the application of the Wiedemann-Franz law.

1-2. The Thermal Magnetoresistance K_{11}. $\Delta K_{11} = K_{11}(H) - K_{11}(0)$ is

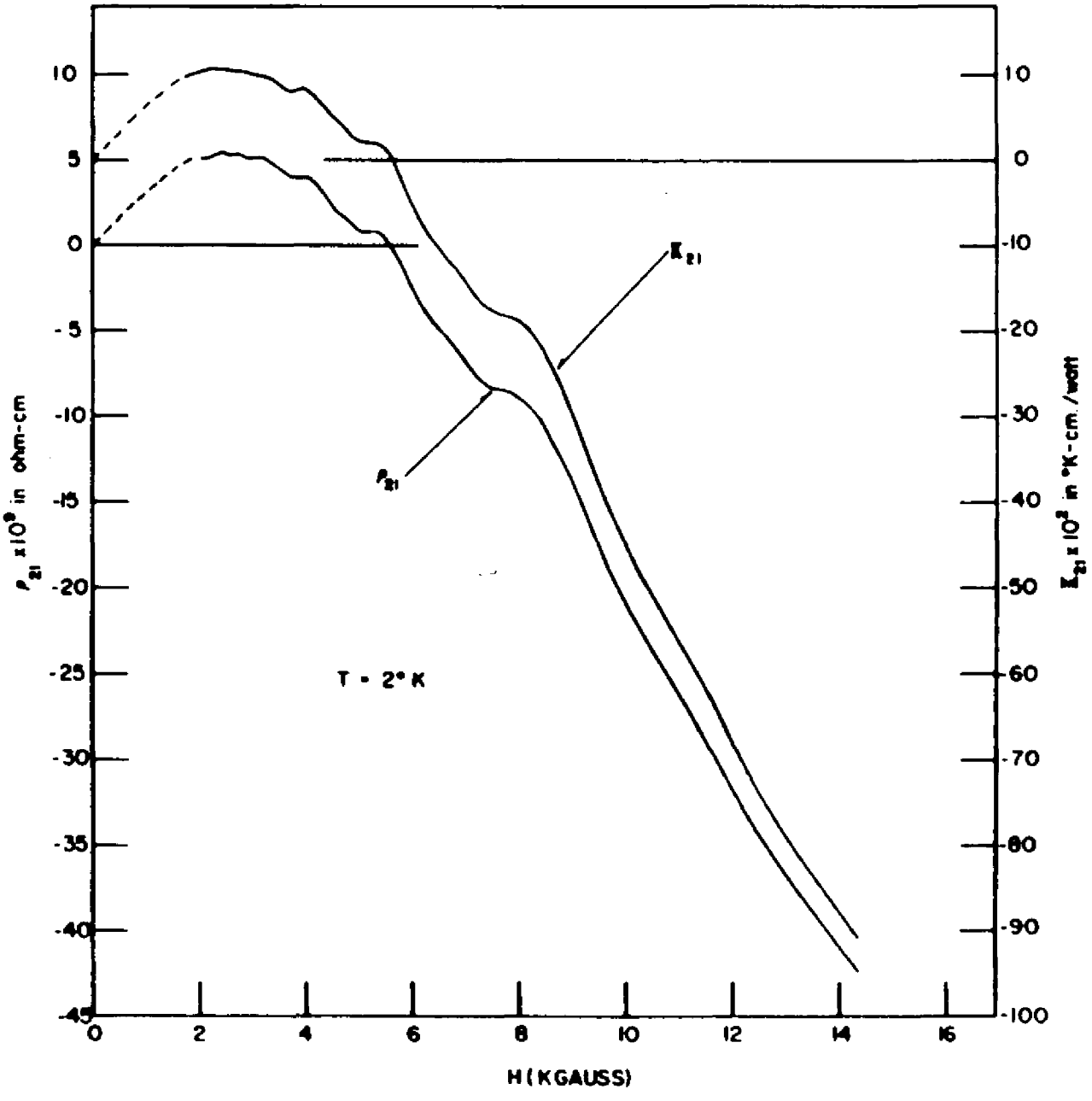
10
5
0
-5
-10
-15
-20
-25
-30
-35
-40
-45
10
0
-10
-20
-30
-40
-50
-60
-70
-80
-90
-100
0
2
4
6
8
10
12
14
16
H(KGAUSS)
T = 2° K
ρ_{21} x10^3 in ohm-cm
E_{21} x 10^3 in °K-cm./watt
E_{21}
ρ_{21}

Fig. 8

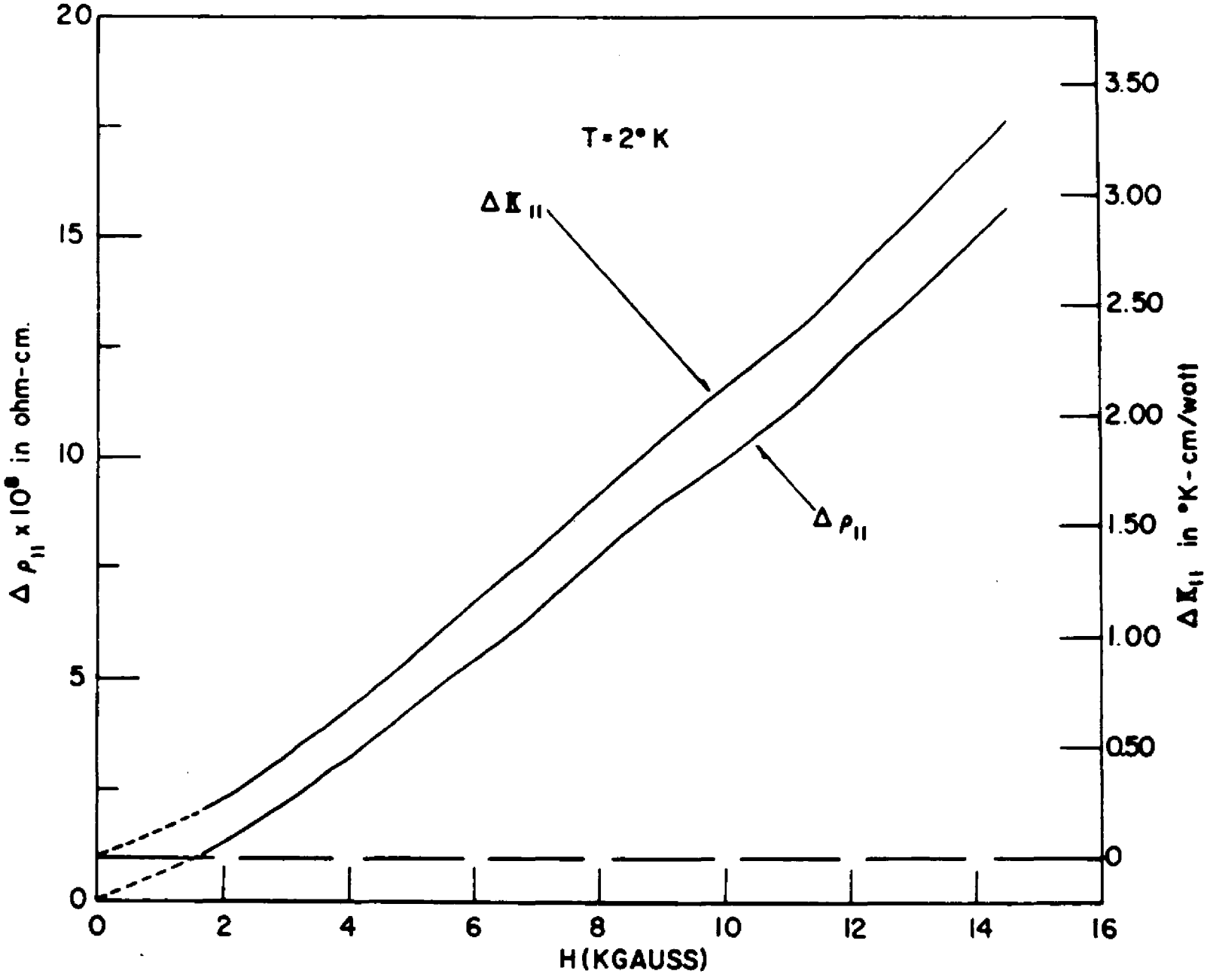
T = 2° K
ΔK_{11}
$\Delta \rho_{11}$
$\Delta \rho_{11}$ x 10^8 in ohm-cm.
ΔK_{11} in °K-cm/watt
H(KGAUSS)
0
5
10
15
20
0
0.50
1.00
1.50
2.00
2.50
3.00
3.50
0
2
4
6
8
10
12
14
16

Fig. 9

represented in Fig. 9, with the plot of the electrical magnetoresistance $\rho_{11} = \rho_{11}(H) - \rho_{11}(0)$ alongside.

If the Wiedemann-Franz law holds at these low temperatures and in presence of the magnetic field, then the change in thermal resistivity should be equal, apart from a constant factor, to the change in electrical resistivity:

$$\frac{\rho_{11}(H)}{K_{11}(H)} = \frac{\rho(0)}{K(0)} = \frac{\rho_{11}(H) - \rho(0)}{K_{11}(H) - K(0)} = L_n T.$$

Plotted in Fig. 9 are $\Delta\rho_{11}$ and ΔK_{11} with the scales adjusted in the ratio $L_n T$. It can be seen that the Wiedemann-Franz law is obeyed, grosso modo, over the entire range of the magnetic field H. The finer details of this comparison will be seen in Fig. 10, where the point by point computation of $L_1' = \frac{\Delta\rho_{11}}{T\Delta K_{11}}$ has been plotted.

2. The Lorenz Ratio

The Lorenz ratio is defined as $L = \frac{\lambda}{\sigma T}$, where λ and σ are the thermal and electrical conductivities respectively. The Wiedemann-Franz law states that L should be a universal constant

$$L_n = \frac{\pi^2}{3}\left(\frac{k}{e}\right)^2 = 2.45 \times 10^{-8} \left(\frac{\text{Volt}}{\text{deg}}\right)^2$$

It will be recalled that a valid measurement of $\lambda_{11}^{-1}(0)$, the residual thermal resistivity, was impossible. This quantity will be determined starting from the residual electrical resistivity $\rho_{11}(0)$, once the validity of the Wiedemann-Franz law has been experimentally established.

2-1. The Longitudinal Apparent Lorenz ratio L_1'. Represented in Fig. 10 are the longitudinal apparent Lorenz ratio L_1'

$$L_1' = \frac{1}{T}\frac{\rho_{11}(H) - \rho_{11}(0)}{K_{11}(H) - K_{11}(0)} = \frac{1}{T}\frac{\Delta\rho_{11}}{\Delta K_{11}}$$

and the transverse apparent Lorenz ratio $L_2' = \frac{1}{T}\frac{\rho_{21}(H)}{K_{21}(H)}$.

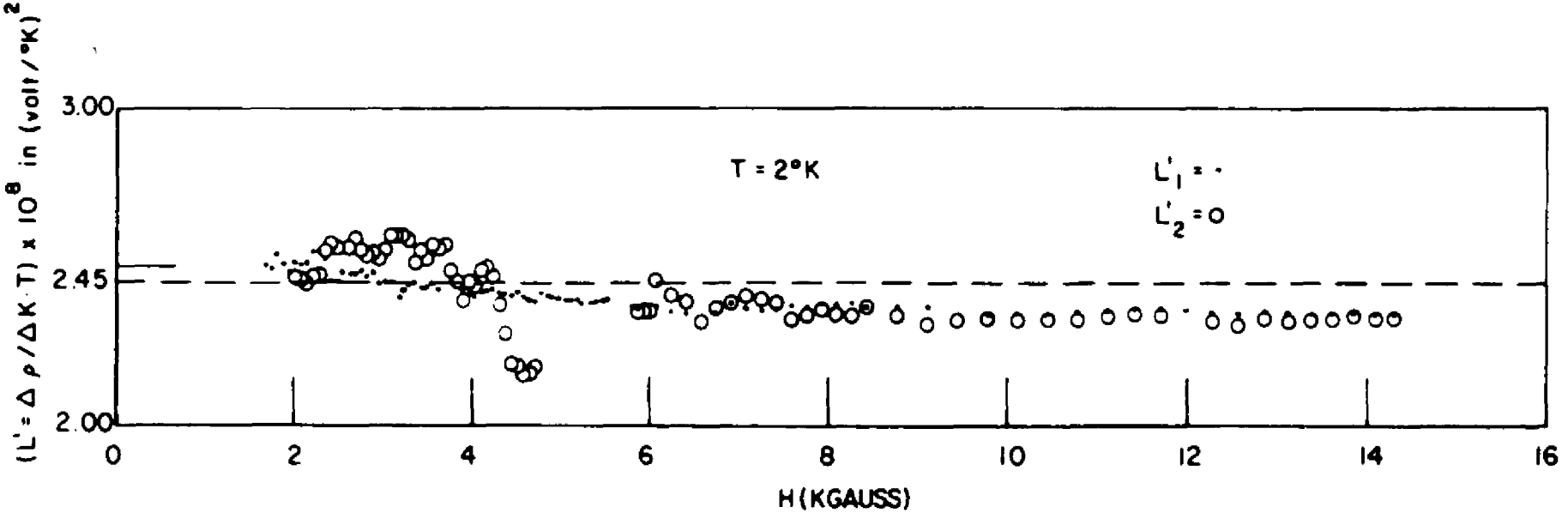
(L' = Δρ/ΔK·T) x 10^8 in (volt/°K)^2
3.00
2.45
2.00
T = 2°K
L'1 = ·
L'2 = 0
0
2
4
6
8
10
12
14
16
H(KGAUSS)

Fig. 10

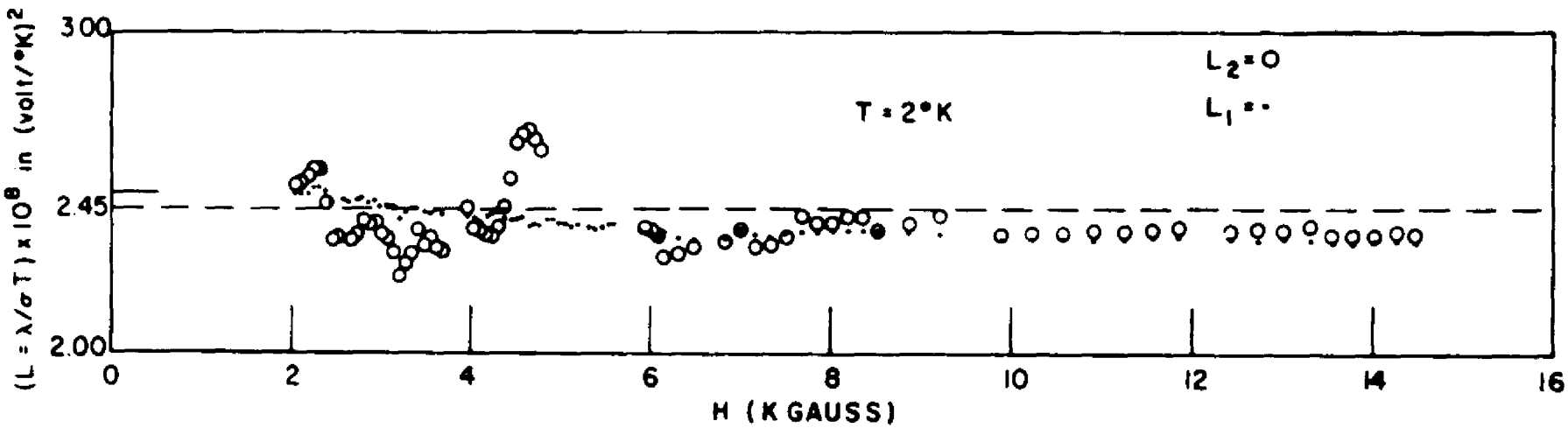
300
2.45
2.00
$(L = \lambda/\sigma T) \times 10^8$ in (volt/°K)^2
$L_2 = 0$
$T = 2°K$
$L_1 = \cdot\cdot$
0
2
4
6
8
10
12
14
16
H (K GAUSS)

Fig. 10a

where $T = 1.98^{\circ}K$.

The plot of L_1', Fig. 10, shows the following features: At relatively low fields i.e. for H between 1.6 and 3.4 kilogauss, L_1' has values larger than L_n by about 3%. With invreasing magnetic field, there is an overall monotonous decrease; finally for values of the field larger than 6 kilogauss L_1' is approximately constant with an average value of $2.35 \times 10^{-8} \left(\frac{volt}{deg}\right)^2$, i.e. $0.96\ L_n$.

It must be noted that the precision of the measurements[13] is better the higher the magnetic field: The effects measured as well as the amplitude of the oscillations become larger when the field increases. The constancy of the Lorenz ratio for fields higher than 6 kilogauss is consequently a result with a very low margin of error.

These results are in complete disagreement with those found by Alers[14] in zinc.

2-2. <u>The Transverse Apparent Lorenz Ratio</u>. This quantity $L_2' = \frac{\rho_{21}^{(H)}}{K_{21}^{(H)}}$ is also plotted in Fig. 10. The values between 4.7 and 5.8 kilogauss were not plotted, because in that region both Righi-Leduc and Hall effects change sign. The values of ρ_{21} and K_{21} are, therefore, close to zero. The experimental errors become relatively very large and the ratio of the two coefficients loses all significance.

The general behavior of L_2' is strikingly similar to that of L_1'. The most important features are the constancy of the values of L_2' for

---

[13] See Appendix I.

[14] P. B. Alers, Phys. Rev. <u>101</u>, 41 (1956).

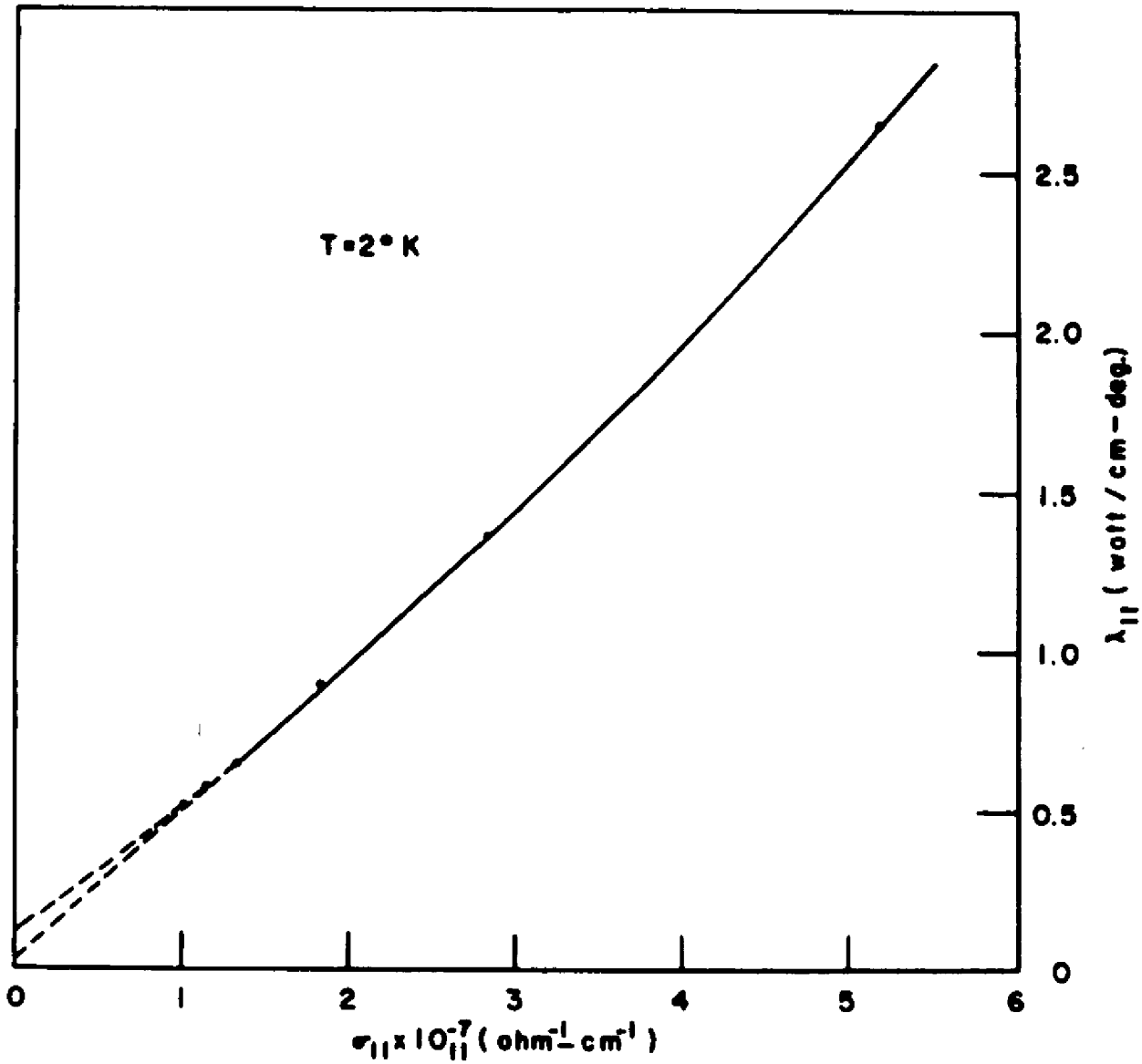
T=2° K
2.5
2.0
1.5
1.0
0.5
0
0
1
2
3
4
5
6
λ_{11} (watt / cm - deg.)
$\sigma_{11} \times 10^{-7}_{11}$ (ohm^{-1} cm^{-1})

Fig 11

magnetic field values larger than 6.5 kilogauss, and the equality of the constant values to which both L_1' and L_2' tend at high field.

It must be borne in mind that these two ratios are computed from two completely different groups of experiments, and this lends further credence to our results. En resumé, we may conclude: (1) both transverse and longitudinal phenomena, in presence of a magnetic field and quantized oscillatory behavior, yield the same Lorenz ratio, for fields larger than 6 kilogauss, at 2°K. (2) This common value stays constant and equal to $2.35 \times 10^{-8} \left(\frac{\text{volt}}{\text{deg}}\right)^2$, when the magnetic field increases from 6 to 14 kilogauss.

2-3. The Lattice Conductivity. The fact that the values of L_1' are close from the free-electron value indicates a priori that the lattice conductivity λ_g zinc at 2°K is very small compared to the electronic conductivity λ_e. A determination of the lattice conductivity can be attempted by writing for the total conductivity $\lambda = \lambda_e + \lambda_g$ where λ_g is assumed to be unaffected by the magnetic field. If λ_e obeys the law of Wiedemann-Franz, $\lambda(H) = \sigma(H)T\, L_e + \lambda_g$, where σ is the electrical conductivity and L_e the Lorenz number for the electronic conductivity which may differ from the normal value L_n.

Let us assume that L_e is unchanged by the magnetic field. Then a plot $\lambda(H)$ versus $\sigma(H)$ is a straight line whose intersection with the vertical axis gives λ_g. No assumption is made about the behavior of σ in very large fields. This method (see Fig. 11) gives a value $\lambda_g = 0.02$ watt/deg-cm at 2°K. The imprecision of the result is due to the lack of high field values, which make the extrapolation rather uncertain. Alers[15] finds by the same method $\lambda_g \tilde{=} 0.5$ but at T = 3.5°K.

---

[15] P.B. Alers, op.cit.

It can be noted here that if the assumption is made that in a perfect lattice the phonons behave like a free-particle gas, this would yield an upper limit value of λ_g. For in this case, one can write[16] $\lambda_g \leq \frac{1}{3} C_v u_o \Lambda$ where C_v is the heat capacity of the lattice waves or phonons, u the velocity of sound and Λ the mean free path of the phonons. At sufficiently low temperatures, the effect of the grain boundary is predominant and we then have $\lambda_g \leq \frac{1}{3} C_v u_o \Lambda_b$ where Λ_b is the smallest dimension of the sample. With the following numerical values: $\Lambda_b \simeq 3 \times 10^{-2}$ cm and $C_v \simeq 12/5\ \pi^4 Nk (\frac{T}{\theta})^3$ with $\theta \sim 308$ for zinc at low temperatures and $u_o \sim 3 \times 10^5$ cm/sec we find $\lambda_g \leq 0.6$ watt/deg-cm for $T = 2^oK$. It should be noted that in this expression the only temperature dependent term is C, the heat capacity, which varies as T^3 at low temperatures. Assuming this T^3 dependence to be valid, one would deduce from Alers' result at 3.5^oK, the value of λ_g at 2^oK. One finds $\lambda_g = 0.09$ watt/deg-cm, which is of the same order than our result.

2-4. Analysis in the Light of the Wilson-Sondheimer Theory.[17] It is well-known that a model based on a single conduction band of normal form leads to vanishing magnetoresistance in first approximation. The two-band model developed by Wilson and Sondheimer is generally used to interpret the experimental results. It consists of two overlapping bands, the s and d bands, and n_1 is to be understood as the number of s electrons while n_2 is the number of vacant d levels.

---

[16] C. Kittel, Solid State Physics, John Wiley and Sons, New York, 2nd edition (1956) p. 143.

[17] A. H. Wilson, Theory of Metals, Cambridge University Press, Cambridge (1953) 2nd edition.

Partial electric conductivities σ_{o1}, σ_{o2} and thermal conductivities λ_{o1} and λ_{o2} are attached to the carriers in band 1 and 2, with zero magnetic field.

From the formulae derived by Wilson[17] for the relative change in electrical resistivity $\Delta\rho/\rho_o$ and thermal resistivity $\Delta K/K_o$, one can deduce the expression for apparent Lorenz number $\frac{\Delta\rho}{\Delta K}\frac{1}{T}$.

The important question is the behavior of the Lorenz number at the limits of zero magnetic field and infinitely large magnetic field. The two-band model predicts that, if L_o is the zero-field limit of the conductivities ratio then two cases can occur (Wilson,[17] page 319): (a) $n_1 = n_2$. When the magnetic field increases from 0 to large values, L increases steadily from L_0 to L_n^2/L_0. (b) $n_1 \neq n_2$. Then L passes through a maximum as H is increased and finally tends to L_0 again.

2-4.1. Limit for H Tending to Zero. By combining the expressions for $\Delta\rho/\rho_0$ and $\Delta K/K_0$, we obtain at the limit of H tending to zero:

$$\text{limit } \frac{\Delta\rho}{\Delta K}\frac{K_0}{\rho_0} = \lim \frac{L_1'}{L_0} = L_n^2 T^2 \frac{\left(\frac{\sigma_{01}}{n_1} + \frac{\sigma_{02}}{n_2}\right)^2 \frac{\sigma_{01}\,\sigma_{02}}{(\sigma_{01} + \sigma_{02})^2}}{\left(\frac{\lambda_{01}}{n_1} + \frac{\lambda_{02}}{n_2}\right)^2 \frac{\lambda_{01}\,\lambda_{02}}{(\lambda_{01} + \lambda_{02})^2}}$$

We have now to make an assumption borne out by an important feature of our results. As shown in Fig. 8, both the Righi-Leduc thermal resistivity and the Hall resistivity change sign at exactly the same value of the magnetic field, $H_0 = 5.58$ kilogauss. In the hypothesis of a two-band model, this would mean $\sigma = \sigma_1 + \sigma_2 = 0$ and $\lambda = \lambda_1 + \lambda_2 = 0$, for $H = H_0$. If one assumes a characteristic Lorenz number attached to

---

[17] A. H. Wilson, Theory of Metals, same as on page 62.

each band $\lambda_1 = TL_1\sigma_1$ and $\lambda_2 = TL_2\sigma_2$ then the above system is compatible only if $L_2 = L_1$ when $H = H_0$. It is reasonable to assume that this equality is also valid for other values of the field including $H = 0$. Therefore,

$$\frac{\lambda_{01}}{\sigma_{01}} = \frac{\lambda_{02}}{\sigma_{02}} = \frac{\lambda_{01} + \lambda_{02}}{\sigma_{01} + \sigma_{02}} = L_0 T$$

It follows that for H tending to zero:

$$\text{limit } \frac{L_1}{L_0} = \left(\frac{L_n}{L_0}\right)^2 \text{, i.e. } \lim L_1 = L_n^2/L_0.$$

The lattice conductivity being negligible at zero field relative to the electronic conductivity, no correction is to be made to the values of L_1', for small fields.

The extrapolation of L_1' to zero field, in Fig. 10, gives $\lim L_1' = 2.58 \times 10^{-8} \left(\frac{\text{volt}}{\text{deg}}\right)^2 = 1.05\ L_n$, i.e. a value larger than L_n by 5%. It must be stressed here that this limit is a different quantity than L_0. For L_0 corresponds to the residual conductivities while L_1' was computed from the field-dependent part of the resistivities.

Comparison of this extrapolated limit with the theoretical one yields:

$$\lim L_1 = \frac{L_n^2}{L_0} = 1.05\ L_n$$

$$L_0 = \frac{L_n}{1.05} = 2.33 \times 10^{-8} \left(\frac{\text{volt}}{\text{deg}}\right)^2$$

As was already pointed out on page 35 the lack of precision in the measurement of K_0 was such that a valid direct determination of this quantity and consequently of L_0 was impossible. Alers[14] has tried to determine it and finds $L_0 = 1.32 \times 10^{-8}$. He must have encountered the same difficulty since he notes that his result is "almost certainly in error." Our value of L_0 is to be used with the value of ρ_0 which is determined with satisfying accuracy at 2°K: $\rho_0 = 4.05 \times 10^{-9}$ ohm-cm. From this, one finds $K_0 = L_0 T \rho_0 = 8.8 \times 10^{-2}$ cm-°K/watt or in terms of

conductivities, at 2°K: $\sigma_0 = 2.47 \times 10^8$ ohm^{-1}cm^{-1} and $\lambda_0 = 11.36$ watt/°K-cm. It is instructive to compare this to Alers' values for his crystal Zn VI, at 3.45°K: $\sigma_0 = 1.23 \times 10^8$ ohm^{-1}cm^{-1} (Alers) and $\lambda_0 = 5.60$ watt-units (Alers).

2-4.2. Limit for H Very Large. In the case $H \neq 0$, under the same assumption, namely:

$$\frac{\lambda_{01}}{\sigma_{01}} = \frac{\lambda_{02}}{\sigma_{02}} = \frac{\lambda_{01} + \lambda_{02}}{\sigma_{01} + \sigma_{02}} = L_0 T$$

one has

$$\frac{L_1}{L_0} = \frac{L_n^2 T^2 + d^2 H^2}{L_0^2 T^2 + d^2 H^2}$$

with

$$d^2 = \frac{(n_1 - n_2)^2}{n_1^2 n_2^2} \quad \frac{\lambda_{01}^2 \lambda_{02}^2}{e^2 c^2 \lambda_0^2}$$

where $\lambda_0 = \lambda_{01} + \lambda_{02}$, $-e$ is the charge of the electron in electrostatic units, and c is the velocity of light. When H varies from zero to very large fields, L_1 changes monotonously from L_n^2/L_0 to L_0 if $n_1 \neq n_2$, or to $\frac{L_n^2}{L_0}$ if $n_1 = n_2$. Our data therefore proves that for zinc, the hypothesis $n_1 \neq n_2$ is the correct one, when the magnetic field is parallel to the hexagonal axis. It is well known that in the case $n_1 \neq n_2$, the magnetoresistance should show a tendency towards saturation. The maximum value of the magnetic field intensity used in this work (14.28 kilogauss) is not high enough to check on this saturation. But Borovik's work[18] (Hmaximum = 25 kilogauss) and Alers' work (Hmaximum = 60 kilogauss) show clearly this saturation, for this particular orientation.

---

[18] E. S. Borovik, Soviet Phys. JETP 3, 243 (1956), trans. from Zhur. Eksptl. i Teoret. Fiz. 30, 262 (1956).

Correction due to lattice conductivity. It is felt that since the lattice conductivity λ_g is of the order of 0.02 watt/cm-deg, i.e. less than 2/1000 of λ_0, the correction at 0 field is negligible. The correction at high field would be more important (a few per cent) but in view of the uncertainty in the value of λ_g, it was thought best not to take it into account.

3. The Peltier and Ettingshausen Coefficient in Zinc

3-1. The results are shown in Figs. 12 and 13. The experimental Peltier coefficient $\pi'_{11} = G_1/J_1$ in deg-cm/amp, i.e. the longitudinal gradient of temperature per unit electric current density is shown on Fig. 12. It possesses a strong monotonic increase with the magnetic field. Oscillations of de Haas-van Alphen type are superimposed on the monotonic variation, with a period of 6.28×10^{-5} gauss^{-1} ± 10% for the high field region H > 4 kilogauss. In a very analogous manner to the behavior of the thermoelectric coefficient ϵ'_{11}, a phase reversal of the oscillations for H < 4 kilogauss is apparent, thus confirming this discovery of Bergeron in his dissertation. Due to the smallness of the effect at low-field values, no precise determination of the low-field periodicity can be attempted. If two envelopes are drawn through the maxima and minima respectively, (taking into account the phase inversion at low fields) and the median points of the envelopes are found, it appears that they lie on a straight line, with a slope of -3.24 deg-cm/amp/kilogauss indicating a linear increase in absolute value of the average of π'_{11} with increasing magnetic field.

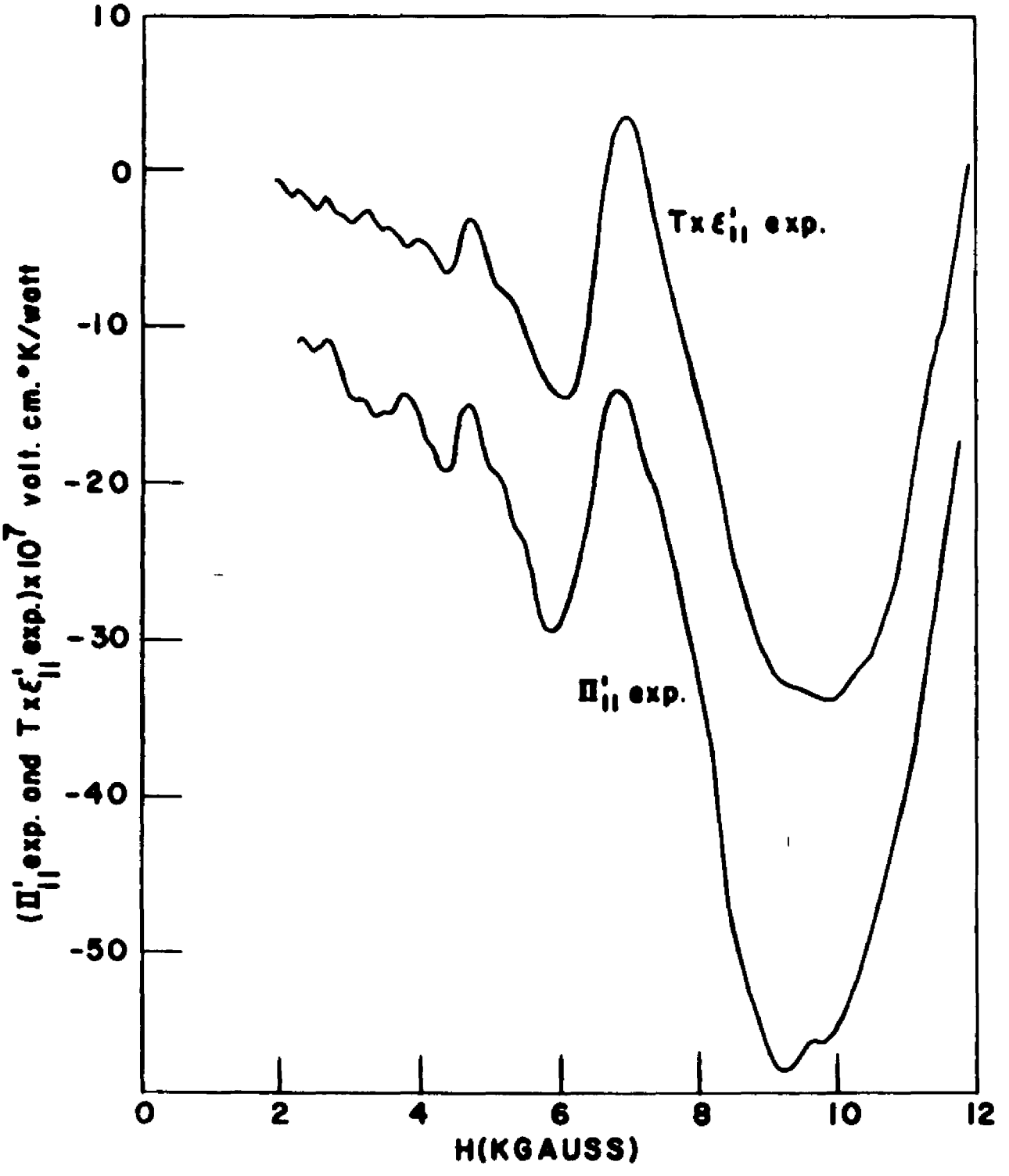

Fig. 12. A Plot of the Measured Thermoelectric Power of Zinc ϵ'_{11} (Multiplied by T) Compared to the Plot of the Measured Peltier Coefficient of Zinc, π'_{11}.

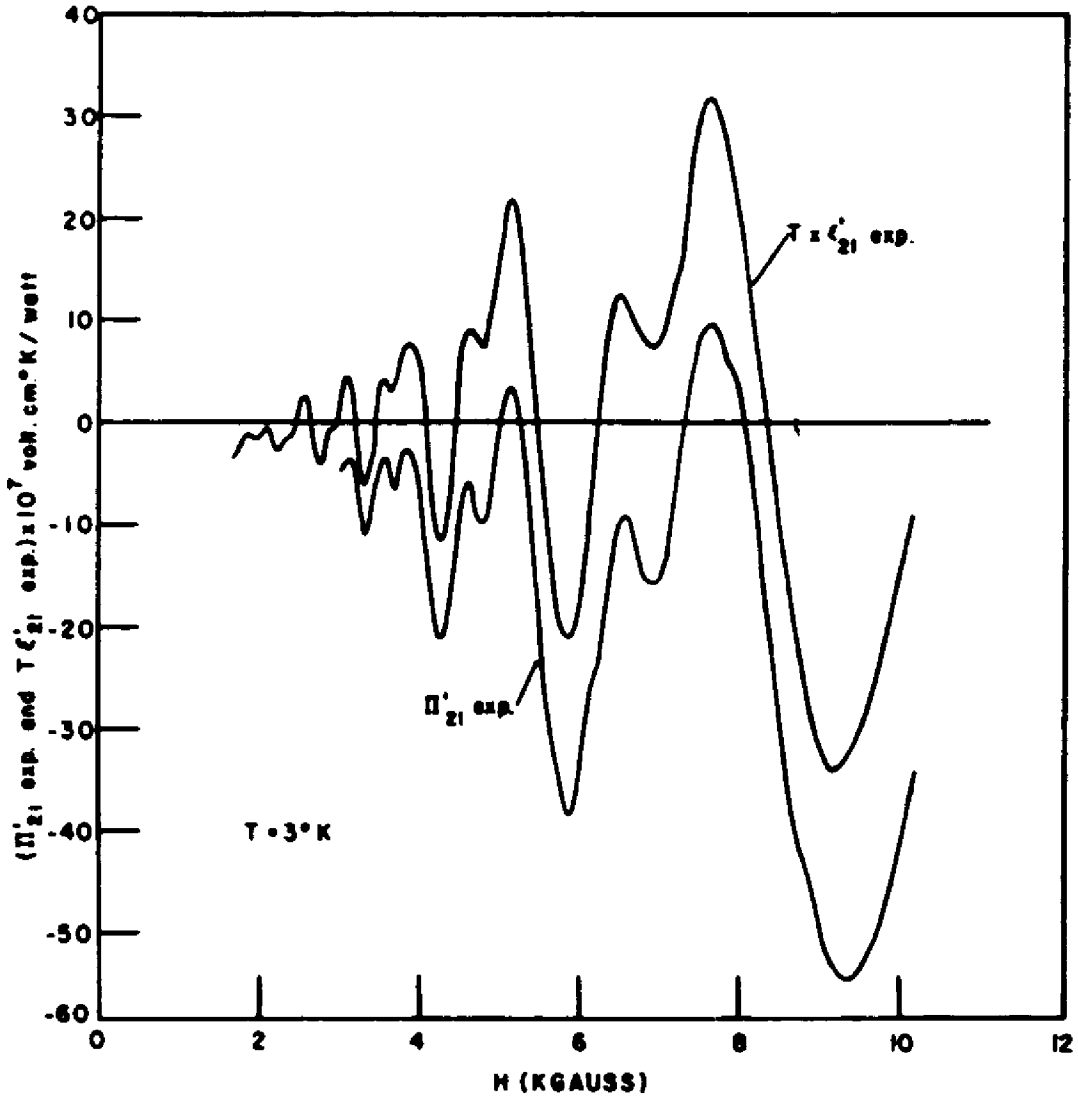

Fig. 13. A Plot of the Measured Nernst-Ettingshausen Coefficient ϵ'_{21} (Multiplied by T) Compared to the Plot of the Ettingshausen Coefficient $-\Pi'_{21}$.

3-2. The experimental Ettingshausen coefficient $\pi'_{21} = G_2/J_1$, i.e the transverse gradient of temperature per unit electric current density is shown in Fig. 13. It is purely oscillatory with a slight monotonic variation that is probably due to a Peltier effect produced by a slight misalignment of the probes. The period of the main oscillations is 6.45×10^{-5} gauss^{-1} ± 10%. The double peak feature, already noted by Bergeron in other thermomagnetic and galvanomagnetic phenomena is present. It is attributed to the existence of a second harmonic of the principal oscillation. The amplitude of the oscillations seem, in first approximation, to increase linearly with the field.

3-3. Analysis in the light of the Onsager theorem.--It was shown that the reciprocal relations of Onsager's theory yield the following relationships between the elements of the Peltier and thermoelectric tensors:

$$\pi'_{11} = T\epsilon'_{11}$$

$$\pi'_{21} = T\epsilon'_{21}$$

where the π'_{ij} and ϵ'_{ij} are the experimentally measured coefficient including implicitly the term due to the presence of the copper leads. Fig. 12 shows the plot of $T\epsilon'_{11}$ * and π'_{11} side by side. The corresponding temperature is T = 2.892°K. The agreement with the Onsager prediction is striking, in the whole field range. It is felt that the displacement that separates the two curves is due to some fortuitous experimental error, probably a variation of the crystal current upon its reversal,

---

*ϵ'_{11} has been computed from the experimental data taken by C. J. Bergeron, using the same crystal.

during the Peltier effect measurement. Much more significant than this discrepancy is the following: If the amplitudes of corresponding oscillations in the two curves, are compared, one finds that they are equal within better than 5%, which is of the order of the experimental errors. Fig. 13 shows the plot of $T\epsilon'_{21}$ and π'_{21} side by side. The corresponding temperature is $T = 2.987^{\circ}K$. The agreement with the Onsager prediction is still closer than in the longitudinal coefficients. The slight displacement between the curves is again felt to be due to fortuitous sources of error. A slight error made on the zero line of π'_{21} for example would explain the discrepancy. The size of the respective oscillations compare at better than 1%. It can be, therefore, stated that Onsager's relations are valid under the extreme conditions of liquid helium temperature, and quantum oscillations, in presence of an external magnetic field. These results bring further credence to the application of Onsager's theory as a tool for analyzing complicated Fermi surfaces in metals.[19]

Experimental determination of $\epsilon'_{11}(0)exp$ and $\pi'_{11}(0)exp$

It was pointed out in the analysis of the experimental procedure that terms ϵ_B and π_B due to the presence of the copper leads was implicitly contained in the experimental quantities ϵ'_{11} and π'_{11}, i.e. the measurement gave $(\epsilon'_{11} - \lambda_{11} - l_{\epsilon B})$ and $(\pi'_{11} - \lambda_{11} - l_{\pi B})$.

In the measurement of the residual values (at zero field) of these quantities, a large factor of imprecision is involved, both because of

---

[19] B. Lax, Rev. of Modern Phys. 30, 122 (1958).

the smallness of these residual effects and because of the rise in temperature that the crystal undergoes when either the heat current or the electric current are turned on.

The measurements gave the following results:

$$\epsilon'_{11}(0) - \lambda_0^{-1}\epsilon_B(0) = -3.9 \times 10^{-8}$$

$$\pi'_{11}(0) - \lambda_0^{-1}\pi_B(0) = +8.3 \times 10^{-7}$$

which are to be considered as very imprecise. The comparison in the light of the reciprocal relation involves then

$$T\epsilon'_{11}(0) \cong -1 \times 10^{-7}$$

$$\pi'_{11}(0) \cong 8.3 \times 10^{-7}$$

In the case of ϵ_B, an approximate value can be found in the paper of Blatt and Kropshot.[20] Their data indicates an extropolated value for "pure" copper

$$\epsilon_B(0) \cong 0.6 \times 10^{-6} \text{ volt/deg}$$

and we find

$$\lambda_0^{-1} = 7.6 \times 10^{-2} \text{ watt/deg-cm}$$

This yields, therefore, $\epsilon'_{11}(0) \cong 0.7 \times 10^{-8}$, a value to be considered as giving only the order of magnitude.

Referring to the lack of precision of the quantities determined above, it can be understood that the experimental measurements were referred to a zero line corresponding to zero field and either heat current or electric current turned on. As a consequence, the values ϵ'_{11exp} and π'_{11exp} plotted in Fig. 12 are in fact equal to:

---

[20] F. J. Blatt and R. H. Kropshot, Phys. Rev. 118, 480 (1960).

$$\epsilon'_{11exp} = \epsilon'_{11} - \lambda_{11}^{-1}\epsilon_B - (\epsilon'_{11}(0) - \lambda_0^{-1}\epsilon_B(0))$$

$$\pi'_{11exp} = \pi'_{11} - \lambda_{11}^{-1}\pi_B - (\pi'_{11}(0) - \lambda_0^{-1}\pi_B(0))$$

In the case of the transverse effects, the experimental curves, Fig. 13, correspond to the theoretical value in a simpler way since it is assumed that both $\pi'_{21}(0)$ and $\epsilon'_{21}(0)$ are null:

$$\epsilon'_{21exp} = \epsilon'_{21} - \lambda_{21}^{-1}\epsilon_B$$

$$\pi'_{21exp} = \pi'_{21} - \lambda_{21}^{-1}\pi_B.$$

It should be pointed out that if the reciprocal relations apply as well to zero field values as to values with field, both in Cu and Zn, then the relation

$$\pi'_{11exp} = T\epsilon'_{11exp}$$

$$\pi'_{21exp} = T\epsilon'_{21exp}$$

is still valid.

3-4. Analysis in the Light of Zil'berman's Theory.[21]

3-4.1. It was found useful to compute from the experimental data the coefficients ϵ''_{11} and ϵ''_{21}. It will be recalled that they are defined by the system of kinetic equations:

$$J = \sigma E^* - \epsilon'' G$$

$$w^* = -\pi'' E^* + \lambda'' G$$

and that they are directly proportional to the number of carriers, whence their importance in a theoretical treatment. The results are plotted in Fig. 14. Some striking features are noticeable.

ϵ''_{21} is purely oscillatory and shows a decrease of the amplitude of the oscillations, at large field ($H > 6$ Kgauss). This is reminiscent

---

[21] G. E. Zil'berman, J. Exptl. Theoret. Phys. U.S.S.R. 29, 762 (1955); Translation, JETP 2, 650 (1956).

of the behavior found by Verkin and Dmitrenko[22] in the magnetic susceptibility in zinc. The period is 6.22×10^{-5} gauss^{-1} for the maxima and 6.35×10^{-5} gauss^{-1} for the minima, at ± 10%.

ϵ''_{11} shows a most interesting behavior. The phase reversal discovered by Bergeron in his dissertation in ϵ'_{11} has disappeared here. There is a monotonic decrease with the field. The irregularity appearing in between the middle peaks is felt to be due to slight variations between the experimental conditions of measurements of the different quantities used to compute ϵ'_{11}. In particular, the computation involves tan , therefore ρ_{11}. This last quantity is extremely dependent on the orientation of the crystal. Hence, a slight variation in the orientation during the measurement of ϵ'_{11} and ϵ'_{21} as compared to that during ρ_{11}, would show under the form of such irregularities.

3-4.2. Zil'berman[23] has derived the expression of the coefficient appearing in

$$J_1 = \sigma_{11} E^* - \epsilon''_{11} G_1$$

For the one band model he finds:

$$\epsilon''_{11} = k^2 T \quad \frac{16\pi^2}{9} E_0 + \frac{\pi^2}{5} \mu H - \frac{40\pi}{kT} E_0^{3/2} e^{-\gamma} (1-\gamma) \sin(9-\tfrac{\pi}{4})$$

under the assumption $e^{\gamma} >> 1$ with $\gamma = 2\pi^2 kT/\mu H$.

The symbols k, T, and μ are the Boltzmann constant, the absolute temperature, and the double effective Bohr magneto respectively, and

$$9 = \frac{2\pi E_0}{\mu H}$$

---

[22] B. I. Verkin and I. M. Dmitrenko, Izvestia Acad. Nauk. U.S.S.R. 29, 409 (1955).

[23] See Appendix 2.

where E_o is the chemical potential, the Fermi energy as measured from the nearest zone boundary. To take into account the whole range of possible values of γ the quantity $e^{\gamma}(1 - \gamma)$ should be replaced, as pointed out by Horton[24] by

$$\frac{1 - \gamma \cosh\gamma}{\sinh \gamma}$$

With the conditions of high magnetic field, and low temperatures, one has $\gamma \ll 1$, for zinc. For γ small, the quantity (1) can be replaced by $-\gamma/3$, so that

$$\epsilon''_{11} = k^2 T \left[\frac{16\pi^2}{g} E_o + \frac{\pi^2}{5} \mu H + \frac{80\pi^3 E_o}{3\mu H}^{3/2} \sin(9 - \pi/4) \right]$$

This predicts a behavior of residual, monotonous and oscillatory parts varying proportionally to T. The experimental facts show that:

1. ϵ'_{ij} is practically independent of T in the liquid helium range.
2. The Wiedemann-Franz law is valid.
3. The resistivity is temperature independent.

Therefore, the relation $\epsilon'' = \sigma \lambda \epsilon' = L_n T \epsilon' \rho^{-2}$ shows that the experimental evidence points to a variation of ϵ''_{11} proportional to T, and, therefore, agree with Zil'berman's prediction. As for the amplitude of the oscillations in ϵ''_{11}, it should decrease for high field as 1/H. It can be noticed that in Fig. 14 the oscillations of ϵ''_{11} seem to tend to a saturation with increasing field. They will decrease at high fields though the lack of points in the high field region makes this

---

[24] P. Horton, private communication.

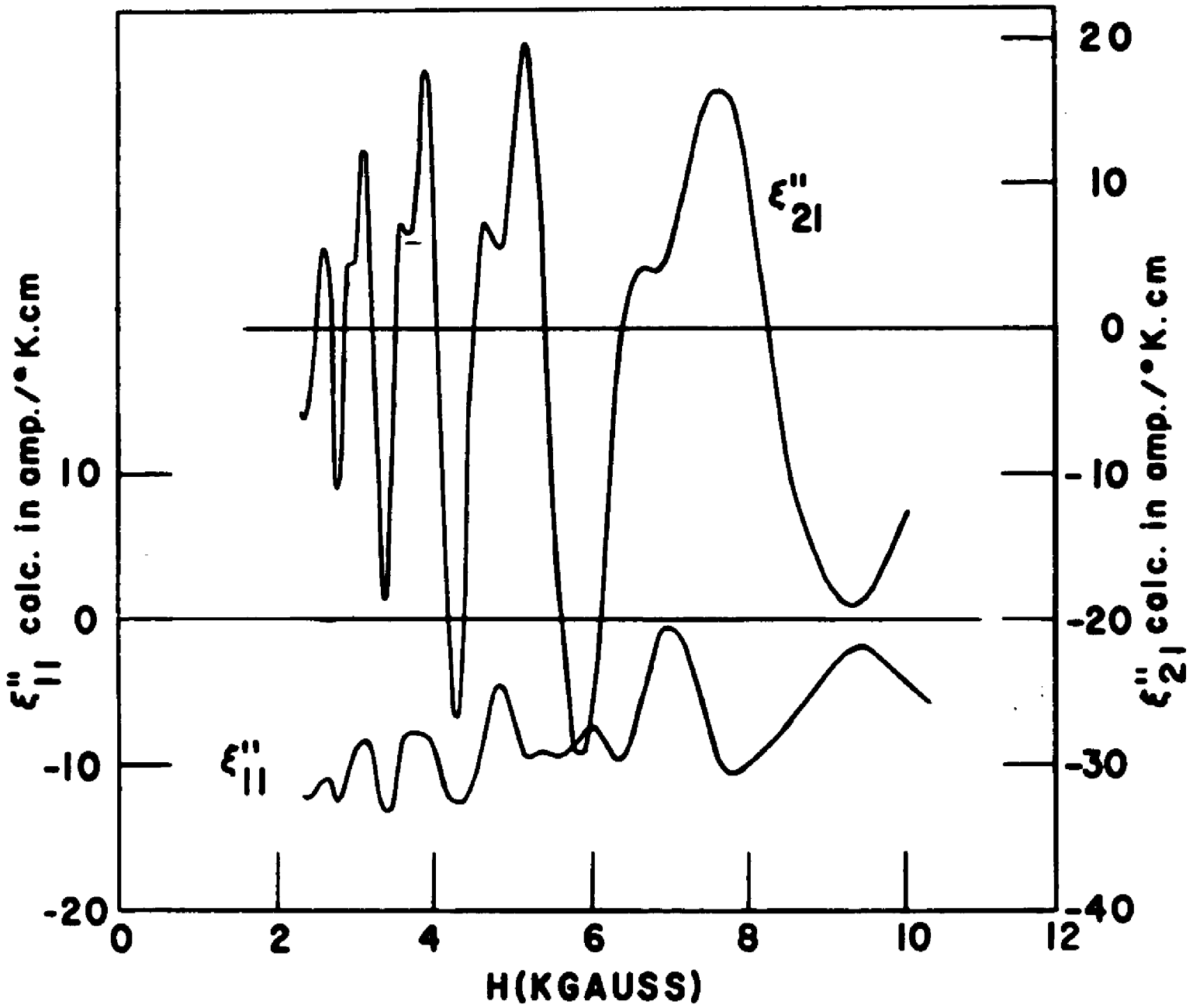

Fig. 14. The Calculated Values of the Longitudinal Thermal Effect ϵ''_{11} and the Transverse Thermal Effect ϵ''_{21}.

affirmation tentative. Finally, Zil'berman's expressions predict a difference of phase of $\pi/2$ between the oscillatory part of σ_{11} and that of ϵ''_{11}. A direct check is not possible, because of the difficulty to determine accurately the oscillations of σ_{11}, as pointed out by Bergeron in his dissertation.

APPENDIX I

Experimental Sources of Error

1. The noise level in the thermometer circuit was higher than in the galvanomagnetic experiments. This would be expected from the introduction of large resistances in the bridge-like measuring circuit. The thermometers themselves have a resistance of about 14 Kohms at 1.6°K, which in itself is an appreciable source of noise.

2. The variations in the dc current furnished by the batteries, estimated at 1% during a single run.

3. The following is an estimate of the accuracy expected for each of the quantities measured.

λ_{21}^{-1} : $\pm 1 \times 10^{-3}$ deg-cm/watt.

λ_{11}^{-1} : $\pm 5 \times 10^{-3}$ deg-cm/watt.

ϵ'_{21} : $\pm 8 \times 10^{-8}$ volt-cm/watt.

π'_{21} : $\pm 14 \times 10^{-8}$ deg-cm/amp.

π'_{11} : $\pm 1 \times 10^{-7}$ deg-cm/amp.

It is clear that these estimates of errors, will yield a high-percentage of error at low-field, where the effects are small, and low-percentage of error at high-field where the amplitude of the effect is large.

Computational Sources of Error

The principal source of error in the computations was involved in the estimation of the temperature difference ΔT equivalent to the voltage signal appearing in the thermometer measuring circuit.

The principle of the computation relied on the fact that any of the ΔT measured was of the order of a few millidegrees. The average temperature of the crystal being determined to a high accuracy, the slope of the corresponding point on the thermometeric calibration curves was used in the computation of ΔT.

The source of error was the fact that at high-field values, the temperature differences cover a larger region than the region in which the slope approximates the curve itself. This involved a quadratic correction and we took special care of it.

The correction was calculated along the following line:

The departure between a curve and its tangent, in the neighborhood of the point of contact, is a quadratic function of the independent variable. The calibration curve of each thermometer is a $V = f(T)$ curve.

If to a voltage deflection X the slope approximation yields a corresponding $(\Delta T)_X$, and if the exact temperature difference is $(\Delta T)_Y$, the voltage deflection should be corrected to ready Y, such that

$$Y = \frac{\partial V}{\partial T} \times (\Delta T)_Y$$

Define a corrective factor by

$$Y = (1 + \epsilon)X$$

then

$$\epsilon = \frac{Y - X}{X}$$

Suppose we determine $\epsilon = \epsilon_1$ for the highest field value H_1. Then at lower values H of the field, the corrective factor will be

$$\epsilon = \epsilon_1 \left(\frac{H}{H_1}\right)^2$$

because of the quadratic nature of the error.

The principal application was in the case of λ_{11}^{-1}, λ_{21}^{-1} and the Lorenz ratios L_1 and L_2.

We had $\epsilon_1 = 0.1432$ for λ_{11}^{-1}.

$\epsilon_1 = 0.1432/4$ for λ_{21}^{-1}.

and for the Lorenz ratios, it followed that:

$$L_1 \text{ corrected} = \frac{L_1 \text{ uncorrected}}{1 + \epsilon}$$

$$L_2 \text{ corrected} = \frac{L_2 \text{ uncorrected}}{} \times (1 - \epsilon/4).$$

APPENDIX II

Data for the calibration curve of the magnetic field:

I (amperes)	H (gauss)	I (amperes)	H (gauss)
5.0	1683	13.0	4377
5.2	1750	13.2	4444
5.4	1818	13.4	4518
5.6	1885	13.6	4579
5.8	1953	13.8	4646
6.0	2020	14.0	4714
6.2	2087	14.2	4781
6.4	2155	14.4	4848
6.6	2222	14.6	4916
6.8	2289	14.8	4983
7.0	2357	15.0	5050
7.2	2424	15.2	5118
7.4	2491	15.4	5185
7.6	2559	15.6	5253
7.8	2626	15.8	5320
8.0	2693	16.0	5387
8.2	2761	16.2	5455
8.4	2828	16.4	5522
8.6	2895	16.6	5589
8.8	2963	16.8	5657
9.0	3030	17.0	5724
9.2	3097	17.2	5791
9.4	3165	17.4	5859
9.6	3232	17.6	5926
9.8	3300	17.8	5993
10.0	3367	18.0	6061
10.2	3434	18.2	6128
10.4	3502	18.4	6195
10.6	3569	18.6	6263
10.8	3636	18.8	6330
11.0	3704	19.0	6397
11.2	3771	19.2	6465
11.4	3838	19.4	6532
11.6	3906	19.6	6599
11.8	3973	19.8	6667
12.0	4040	20.0	6734
12.2	4108	20.5	6902
12.4	4175	21.0	7071
12.6	4242	21.5	7239
12.8	4310	22.0	7407

I (amperes)	H (gauss)	I (amperes)	H (gauss)
22.5	7576	29.5	9933
23.0	7744	30.0	10101
23.5	7912	32.5	10960
24.0	8081	35.0	11700
25.0	8417	37.5	12440
25.5	8585	40.0	13130
26.0	8754	45.0	14280
26.5	8923	50.0	15270
27.0	9091	60.0	16550
27.5	9259	70.0	17300
28.0	9428	80.0	17850
28.5	9596	90.0	(18250)

NOTE: The data listed above for $\Delta\lambda_{11}^{-1}$ and λ_{21}^{-1} was collected by N.H. Zebouni in the October, 1960, in the run classified "Louise." The data for $\Delta\rho_{11}$ and ρ_{21} was similarly collected in the run classified "Maria."

Numerical data corresponding to Figs. 8, 9, and 10:

I Amperes	$\Delta_{11}^{-1}\times10^{-2}$ °K-cm/watt	$\rho_{21}^{-1}\times10^{2}$ °K-cm/watt	$\Delta\rho_{11}\times10^{10}$ ohm-cm	$\rho_{21}\times10^{9}$ ohm-cm	$L_1\times10^{8}$ (volt/deg)^2	$L_2'\times10^{8}$ (volt/deg)^2
5	20.90	+ 9.59	104.56	---	2.500	-----
6	26.32	+ 10.26	132.36	+ 5.07	2.514	2.468
7	32.43	+ 10.55	163.41	+ 5.38	2.520	2.550
8	39.45	+ 10.34	195.12	+ 5.35	2.473	2.587
9	46.26	+ 10.02	226.74	+ 5.12	2.45	2.553
10	53.76	+ 9.38	262.88	+ 4.71	2.445	2.511
11	61.50	+ 7.94	------	+ 4.08	-----	2.566
12	68.81	+ 7.92	331.01	+ 3.86	2.405	2.437
13	76.35	+ 5.65	368.18	+ 2.59	2.411	2.290
14	84.82	+ 3.76	405.35	+ 1.64	2.390	2.180
15	93.08	+ 2.11	445.24	+ 0.79	2.392	1.860
16	101.35	+ 1.52	484.25	+ 0.66	2.389	2.16
17	------	- 1.99	521.78	- 0.90	-----	2.26
18	117.95	- 6.54	559.67	- 3.21	2.373	2.455
19	126.37	- 9.87	594.49	- 4.72	2.352	2.390
20	134.02	- 12.35	631.66	- 5.86	2.357	2.370
21	142.45	- 15.30	673.53	- 7.36	2.364	2.404
22	151.17	- 17.44	716.72	- 8.32	2.371	2.386
23	160.32	- 18.42	760.76	- 8.65	2.373	2.347
24	168.77	- 19.80	805.46	- 9.31	2.386	2.350
25	177.63	- 22.71	844.51	-10.78	2.377	2.373
26	186.28	- 26.91	884.60	-12.63	2.375	2.346
27	193.83	- 32.45	919.97	-15.05	2.373	2.319
28	------	- 37.70	953.48	-17.58	-----	2.332
29	209.82	- 42.71	986.13	-19.94	2.350	2.334
30	217.83	- 47.01	1024.30	-21.91	2.351	2.330
35	258.03	- 65.22	1221.80	-30.57	2.367	2.344
40	298.01	- 80.94	1406.30	-37.65	2.360	2.326
45	333.70	- 90.96	1570.00	-42.48	2.352	2.335

Numerical data for Figs. 12 and 13:

I Amperes	$\epsilon'_{11} \times 10^8$ Volt-cm/watt	$\epsilon'_{21} \times 10^7$ Volt-cm/watt	$\pi'_{11} \times 10^7$ cm-°K/amp	$\pi'_{21} \times 10^7$ cm-°K/amp
5	------	-1.20	- 8.85	------
6	- 2.46	-1.69	-12.89	------
7	- 4.83	-1.63	-10.84	- 6.85
8	- 7.61	-1.32	-11.28	- 7.44
9	-10.64	-2.83	-13.94	- 4.64
10	- 9.25	-2.99	-15.49	- 9.01
11	-13.51	-2.25	-15.38	- 6.47
12	-15.80	-0.86	-15.27	-12.29
13	-21.61	-3.86	-19.30	-15.97
14	-13.42	-6.65	-15.32	- 9.65
15	-21.12	-3.07	-19.08	+ 2.69
16	-28.65	+2.83	-22.84	-13.38
17	-42.40	+0.68	-28.54	-35.28
18	-50.50	-4.68	-----	-27.13
19	-40.76	-4.02	-23.06	-12.08
20	- 3.27	-4.90	-14.93	-15.00
21	+10.97	-8.88	-15.10	- 9.44
22	- 9.09	-8.76	-20.24	+ 6.85
23	-33.07	-4.50	-27.05	+ 5.93
24	-53.45	+0.66	-34.96	- 4.21
25	-76.78	+4.24	-47.57	-28.90
26	-100.00	+6.21	-53.82	-43.32
27	-112.3	+5.42	-57.58	-53.39
28	-115.3	+3.03	-56.64	-53.29
29	-117.3	-0.16	-55.97	-45.03
30	-115.1		-53.37	-33.17
31			-48.29	
32			-44.03	
33			-34.51	

NOTE: The values of ϵ'_{11} listed here are from experimental data collected by C. J. Bergéron in 1959, namely, his runs classified SK2k and SK2j. The values of ϵ'_{21} listed here are from experimental data collected by N. H. Zebouni[21] in the Spring, 1960, namely his run classified "Helen." Similarly, π'_{11} and π'_{21} were collected by N. H. Zebouni, Spring, 1960, in the runs classified Kiki 1 and 2.

Numerical data for computation of the coefficients of Fig. 14:

I Amperes	$\lambda_{21} \times 10$ °K-cm/watt	$\lambda_{11} \times 10$ °K-cm/watt	$\epsilon'_{21} \times 10^8$ Volt-cm/watt	$\epsilon'_{11} \times 10^8$ Volt-cm/watt	$\sigma_{21} \times 10^{-6}$ $ohm^{-1}-cm^{-1}$	$\sigma_{11} \times 10^{-6}$ $ohm^{-1}-cm^{-1}$
5	-10.18	+30.95				
6	- 7.88	26.58	-	- 2.46	-15.62	+53.28
7	- 5.97	23.03	- 7.69	- 4.83	-12.10	45.85
8	- 4.34	20.02	- 2.57	- 7.61	- 9.16	40.36
9	- 3.26	17.74	+ 3.25	- 10.64	- 6.90	36.10
10	- 2.38	15.76	- 25.69	- 9.25	- 5.00	32.20
11	- 1.61	14.15	+ 6.85	- 13.51	----	-----
12	- 1.32	12.84	- 4.28	- 15.80	- 2.77	26.63
13	- 0.786	11.77	- 46.20	- 21.61	- 1.54	24.37
14	- 0.433	10.73	+ 14.97	- 13.42	- 0.822	22.40
15	- 0.205	9.86	+ 43.63	- 21.12	- 0.334	20.58
16	- 0.127	9.12	+ 5.14	- 28.65	- 0.239	19.05
17	-----	----	-100.97	- 42.40	+ 0.884	17.78
18	+ 0.409	7.90	- 70.33	- 50.50	+ 0.889	16.62
19	+ 0.542	7.39	+ 15.40	- 40.76	+ 1.163	15.66
20	+ 0.605	6.97	+ 27.38	- 3.27	+ 1.288	14.77
21	+ 0.666	6.57	+ 46.37	+ 10.97	+ 1.428	13.85
22	+ 0.678	6.20	+109.69	- 9.09	+ 1.434	13.05
23	+ 0.640	5.86	+128.36	- 33.07	+ 1.331	12.34
24	+ 0.624	5.58	+ 61.18	- 53.45	+ 1.285	11.68
25	+ 0.648	5.30	- 41.06	- 76.78	+ 1.357	11.13
26	+ 0.697	5.04	-125.79	-100.00	+ 1.448	10.61
27	+ 0.775	4.82	-164.70	-112.3	+ 1.593	10.16
28	-----	----	-155.73	-115.3	+ 1.725	9.75
29	+ 0.864	4.41	-108.50	-117.3	+ 1.823	9.39
30	+ 0.881	4.24	- 46.63	-115.1	+ 1.854	9.01
35	+ 0.868	3.54	- 8.56		+ 1.812	7.48
40	+ 0.807	3.05	+ 23.95		+ 1.684	6.47
45	+ 0.726	2.73	+ 49.62		+ 1.531	5.80

NOTE: The data listed above for ϵ'_{21} and ϵ'_{11} was collected by C.G. Bergeron in 1959 in his runs classified γK2i (ϵ'_{21}) and SK2k and SK2j (ϵ'_{11}). The values for λ_{21} and λ_{11} were computed from data collected by N.H. Zebouni in October, 1960, in the run classified "Maria." The values for σ_{21} and σ_{11} were computed from data collected by N.H. Zebouni in October, 1960, in the run classified "Louise."

SELECTED BIBLIOGRAPHY

Alers, P. B., Phys. Rev. 101, 41 (1956).

Ali, S. A., Dissertation, Louisiana State University (1958); unpublished.

Bergeron, C. J., Dissertation, Louisiana State University (1959); unpublished.

Blatt, F. J. and R. H. Kropshot, Phys. Rev. 118, 480 (1960).

Clement, J. R. and E. H. Quinnell, Rev. Sci. Instr. 23, 213 (1952).

Callen, H. B., Thermodynamics, John Wiley and Sons, Inc. New York, 1960.

Callen, H. B., Phys. Rev. 73, 1349 (1948); 85, 16 (1952).

Jan, J. P., in Solid State Physics, Vol 5, F. Seitz and D. Turnbull, editors, Academic Press, Inc., New York, 1957.

Kohler, M., Ann. Physik 40, 601 (1941).

Kittel, C., Solid State Physics, John Wiley and Sons, New York 2nd ed. (1956).

Mazur, P. and I. Prigogine, J. Phys. Radium, 12, 616 (1951).

de Nobel, J., Physica 15, 532 (1949); 23, 261, 349 (1957).

Onsager, L., Phys. Rev. 37, 405 (1931); 38, 2265 (1931).

Verkin, B. I. and I. M. Dmitrenko, Izvestia Acad. Nauk. U.S.S.R. 29, 409 (1955).

Wilson, A. H., Theory of Metals, Cambridge University Press, Cambridge, 2nd ed. (1953).

Zil'berman, G. E., J. Exptl. Theoret. Phys. U.S.S.R. 29, 762 (1955); translation, JETP 2, 650 (1956).

VITA

Nadim H. Zebouni was born in Beirut, Lebanon, on April 14, 1928. He graduated from the International College of the American University of Beirut in July, 1945. He subsequently entered the Sorbonne, Paris, France, where he was awarded a B.Sc. in Physics (Hon.) in 1953. In 1955 he graduated in Telecommunication Engineering from the Ecole Nationale Superieure des Telecommunications, Paris, France. In 1956-1957 he was engineering Delegate of the Compagnie Generale de T.S.F., Paris, to the Middle East. In September, 1957, he entered the Graduate School of Louisiana State University with a teaching assistanship in the Physics Department. He is now a candidate for the degree of Doctor of Philosophy in the Department of Physics and Astronomy.

EXAMINATION AND THESIS REPORT

Candidate: Nadim Hanna Zebouni

Major Field: Physics

Title of Thesis: The Thermal Conductivity and Peltier Tensors in Zinc at Low Temperatures

Approved:

J. M. Reynolds
Major Professor and Chairman

Richard L. Russell
Dean of the Graduate School

EXAMINING COMMITTEE:

B G Mitchell

George W. Morris.

D C Rapp

Claude J Grenier

Date of Examination:

July 29, 1960